
RIFT: Closed-Loop RL Fine-Tuning for Realistic and Controllable Traffic Simulation

Keyu Chen¹ Wenchao Sun¹ Hao Cheng¹ Sifa Zheng¹

¹ School of Vehicle and Mobility, Tsinghua University

Abstract

Achieving both realism and controllability in interactive closed-loop traffic simulation remains a key challenge in autonomous driving. Data-driven simulation methods reproduce realistic trajectories but suffer from *covariate shift* in closed-loop deployment, compounded by simplified dynamics models that further reduce reliability. Conversely, physics-based simulation methods enhance reliable and controllable closed-loop interactions but often lack expert demonstrations, compromising realism. To address these challenges, we introduce a dual-stage AV-centered simulation framework that conducts open-loop imitation learning pre-training in a data-driven simulator to capture trajectory-level realism and multimodality, followed by closed-loop reinforcement learning fine-tuning in a physics-based simulator to enhance controllability and mitigate covariate shift. In the fine-tuning stage, we propose *RIFT*, a simple yet effective closed-loop RL fine-tuning strategy that preserves the trajectory-level multimodality through a GRPO-style group-relative advantage formulation, while enhancing controllability and training stability by replacing KL regularization with the dual-clip mechanism. Extensive experiments demonstrate that *RIFT* significantly improves the realism and controllability of generated traffic scenarios, providing a robust platform for evaluating autonomous vehicle performance in diverse and interactive scenarios. Project Page: <https://currychen77.github.io/RIFT/>

1 Introduction

Reliable closed-loop traffic simulation is critical for developing advanced autonomous driving systems, supporting training and evaluation [1, 2]. An ideal simulation should possess two key properties: *realistic*, reflecting real-world driving behavior; *controllable*, enabling customizable interaction styles. Existing studies typically focus either on generating realistic traffic scenarios [3, 4] or on constructing controllable interactions [5–7]. Jointly ensuring realism and controllability in interactive closed-loop scenarios remains an open problem.

Traffic simulation approaches can be broadly categorized based on the underlying simulation platform, each presenting distinct trade-offs between realism and controllability, as illustrated in Figure 1. Methods based on data-driven simulators exploit real-world data to generate realistic trajectories by learning multimodal behavioral patterns through imitation learning (IL), conditioned on the initial scene context [8, 9]. However, their open-loop training paradigm introduces the *covariate shift* problem during closed-loop deployment, arising from the distribution mismatch between training and deployment states. Moreover, data-driven simulators often adopt a unified vehicle dynamics model for all agents and simplified environment dynamics [10, 11], resulting in unrealistic interactions and state transitions that further degrade closed-loop reliability. In contrast, physics-based simulators provide fine-grained control over scenario configuration through physical engines, enabling high-fidelity closed-loop interactions. Nonetheless, the absence of expert demonstrations makes it challenging to reproduce realistic behavior. To mitigate this, several approaches employ reinforcement learning

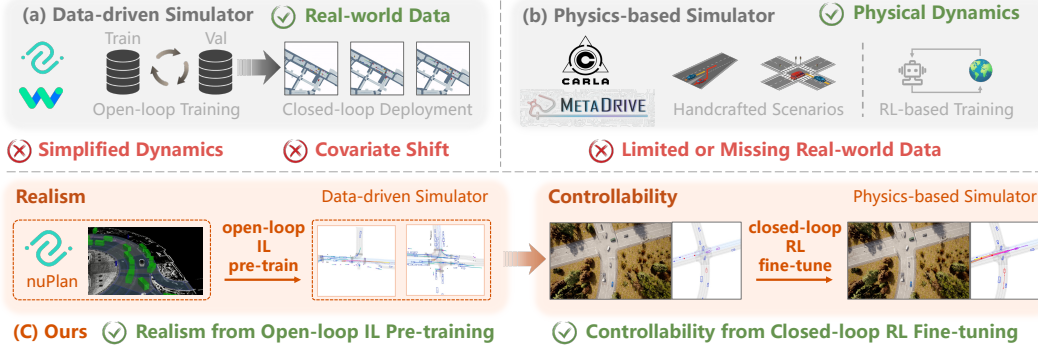


Figure 1: **Traffic Simulation across Different Platforms.** (a) Data-driven Simulator: employs imitation learning to replicate real-world driving behaviors, but suffers from covariate shift and simplified dynamics; (b) Physics-based Simulator: enables controllable scenario construction via high-fidelity closed-loop interaction, but lacks large-scale real-world data; (c) Our framework: combines open-loop IL pre-training in a data-driven simulator to ensure realism with closed-loop RL fine-tuning in a physics-based simulator to enhance controllability.

(RL) to acquire controllable behaviors directly through interaction with the simulator [12–15], though often at the cost of realism. Other approaches enhance realism by injecting real-world traffic data into physics-based simulators [16, 17], but typically rely on log-replay or rule-based simulation, limiting controllability and interactivity. Despite recent advances, a fundamental trade-off persists between realism and controllability across both paradigms, making it challenging to achieve both simultaneously in interactive closed-loop scenarios.

Drawing inspiration from the widely adopted “pre-training and fine-tuning” paradigm in large language models (LLMs) [18–20], we combine the strengths of two traffic simulation paradigms. Specifically, we perform open-loop IL pre-training in a data-driven simulator to capture trajectory-level realism and multimodality, followed by closed-loop RL fine-tuning in a physics-based simulator to address covariate shift and enhance controllability in interactive scenarios.

Building on this foundation, we introduce a dual-stage AV-centered simulation framework, as illustrated in Figure 1, which integrates the strengths of both data-driven and physics-based simulators through the “pre-training and fine-tuning” paradigm, thereby balancing realism and controllability in traffic simulation. Within this framework, critical background vehicles (CBVs) are first identified via route-level interaction analysis to construct interactive scenarios, focusing on agents most likely to interact with the AV. We then leverage an IL pre-trained trajectory generation model to produce multimodal and realistic CBV trajectories, ensuring trajectory-level realism. In the fine-tuning stage, we propose *RIFT*, a simple yet effective closed-loop RL fine-tuning strategy designed to enhance controllability and mitigate covariate shift. While previous approaches [21, 22] typically fine-tune only the best-performing trajectory or action, *RIFT* evaluates all candidate trajectories using a GRPO-style [20] group-relative advantage, preserving trajectory-level multimodality during fine-tuning. Additionally, by replacing KL regularization with a dual-clip surrogate objective, *RIFT* improves controllability and training stability in highly interactive closed-loop scenarios. Our contributions can be summarized as:

- We propose a dual-stage AV-centered simulation framework that combines open-loop IL pre-training in a data-driven simulator to capture trajectory-level realism and multimodality with closed-loop RL fine-tuning in a physics-based simulator to enhance controllability and mitigate covariate shift. This decoupled paradigm leverages the complementary strengths of both platforms, balancing realism and controllability in interactive closed-loop scenarios.
- We propose *RIFT*, a simple yet effective closed-loop RL fine-tuning strategy that enhances controllability and mitigates covariate shift in interactive closed-loop scenarios. During fine-tuning, *RIFT* maintains trajectory-level multimodality via a GRPO-style group-relative advantage formulation while enhancing controllability and training stability by replacing KL regularization with a dual-clip surrogate objective.
- Extensive experiments demonstrate that *RIFT* enables the generation of realistic and controllable scenarios, and improves the reliability of AV evaluation under diverse and interactive scenarios.

2 Related Work

Realistic Traffic Simulation. A variety of generative architectures have been explored for realistic traffic simulation, including conditional variational autoencoders [23–25] and diffusion-based models [26–28]. However, maintaining long-term stability remains challenging due to the *covariate shift* between open-loop training and closed-loop deployment. Recent methods such as SMART [29], GUMP [30], Trajeglish [31], and MotionLM [32] address this issue by formulating traffic simulation as a next-token prediction (NTP) task, leveraging discrete action spaces to improve closed-loop robustness. Despite these advances, most approaches remain confined to data-driven simulation platforms [10, 11, 33, 34], which typically adopt a uniform vehicle dynamics model across agents and simplified environmental dynamics. Such oversimplifications limit the fidelity and reliability of long-term closed-loop interactions, especially in complex and interactive scenarios.

Controllable Traffic Simulation. To generate traffic scenarios aligned with user intent, recent studies have introduced diverse conditioning mechanisms. CTG [35] and MotionDiffuser [36] employ diffusion models conditioned on cost-based control signals. Language-conditioned methods, including CTG++[37], LCTGen[38], and ProSim [39], enable user specification through natural language prompts. Other strategies adopt guided sampling (SceneControl [40]), retrieval-based generation (RealGen [41]), or reward-driven causality modeling (CCDiff [42]). Though effective in improving controllability, these approaches are typically limited to open-loop or simplified environments, leaving the challenge of unifying realism and controllability in closed-loop simulation unresolved.

Closed-Loop Fine-Tuning. Covariate shift—the mismatch between open-loop training and closed-loop deployment—remains a key challenge for reliable long-term traffic simulation. To address this, recent work explores closed-loop fine-tuning strategies. Hybrid IL and RL methods [21, 22, 43] enhance robustness but typically fine-tune the entire model via RL, which often compromises realism due to the difficulty of designing human-aligned reward functions. Supervised fine-tuning approaches such as CAT-K [44] show strong performance but rely on expert demonstrations, limiting scalability. TrafficRLHF [45] improves alignment through reinforcement learning with human feedback (RLHF), but demands costly human input and suffers from reward model instability. Moreover, most existing methods focus on optimizing the best action or trajectory, ignoring the inherent multimodality of traffic simulation, thus limiting behavioral diversity during fine-tuning.

3 Background

3.1 Task Redefinition

Following the widely adopted paradigm for closed-loop evaluation and training in autonomous driving [46, 47], our simulation framework includes a single autonomous vehicle (AV) navigating a predefined global route, accompanied by multiple rule-based background vehicles (BVs), forming an AV-centered closed-loop simulation environment. These BVs either provide diverse interactive data for training or serve to evaluate the AV’s robustness. Building upon this setup, we identify a subset of critical background vehicles (CBVs) that exhibit a higher likelihood of interacting with the AV. For these CBVs, the rule-based control is replaced with a well-trained trajectory generation model, enabling the synthesis of realistic and controllable behaviors in interactive closed-loop scenarios.

3.2 CBV-Centered Realistic Trajectory Generation

With recent advances in imitation learning, data-driven approaches have demonstrated strong performance in generating realistic, multimodal trajectories [48–52]. In fully observable simulation environments, methods like Pluto [53] can generate more reliable trajectories by leveraging ground-truth states. Moreover, its modular encoder-decoder architecture also facilitates downstream fine-tuning. Based on these advantages, we adopt Pluto as our trajectory generation model for synthesizing realistic, multimodal trajectories. Implementation details are presented below.

CBV-Centered Scene Encoding. Following [53], for each CBV in the scene, we extract its current feature F_{cbv} , the historical features of neighboring vehicles F_{neighbor} , and vectorized map features F_{map} . These features are encoded into $E_{\text{cbv}} \in \mathbb{R}^{1 \times D}$, $E_{\text{neighbor}} \in \mathbb{R}^{N_{\text{neighbor}} \times D}$, and $E_{\text{map}} \in \mathbb{R}^{N_{\text{map}} \times D}$, respectively, where N_{neighbor} and N_{map} denote the number of neighboring vehicles and map elements, and D is the embedding dimension. To model the interactions among these

embeddings, we concatenate them and apply a global positional embedding (PE) to obtain the unified scene embedding $E_s \in \mathbb{R}^{(1+N_{\text{neighbor}}+N_{\text{map}}) \times D}$ as:

$$E_s = \text{concat}(E_{\text{cbv}}, E_{\text{neighbor}}, E_{\text{map}}) + \text{PE}. \quad (1)$$

This scene embedding E_s is then passed through N Transformer encoder blocks for feature aggregation, yielding the final CBV-centered scene embedding E_{enc} . Each encoder block follows the standard Transformer formulation. Specifically, the i -th block is defined as:

$$\begin{aligned} E_s^i &= E_s^{i-1} + \text{MHA}(\text{LayerNorm}(E_s^{i-1})), \\ E_s^i &= E_s^i + \text{FFN}(\text{LayerNorm}(E_s^i)), \end{aligned} \quad (2)$$

where MHA is the standard multi-head attention function, FFN is the feedforward network layer.

Multimodal Trajectory Decoding. To capture the multimodal nature of real-world driving behaviors, we adopt the longitudinal-lateral decoupling mechanism proposed in [53]. This approach leverages reference line information to construct high-level lateral queries $Q_{\text{lat}} \in \mathbb{R}^{N_{\text{ref}} \times D}$, and introduces learnable longitudinal queries $Q_{\text{lon}} \in \mathbb{R}^{N_{\text{lon}} \times D}$. These are concatenated and projected to form the multimodal navigation query $Q_{\text{nav}} \in \mathbb{R}^{N_{\text{ref}} \times N_{\text{lon}} \times D}$ as:

$$Q_{\text{nav}} = \text{Projection}(\text{concat}(Q_{\text{lat}}, Q_{\text{lon}})), \quad (3)$$

where N_{ref} and N_{lon} denote the number of reference lines and longitudinal anchors, respectively. The navigation query Q_{nav} and the scene embedding E_{enc} are then fed into N decoder blocks to model lateral, longitudinal, and cross-modal interactions. Each decoder block is structured as:

$$\begin{aligned} \hat{Q}_{\text{nav}}^{i-1} &= \text{SelfAttn}(\text{SelfAttn}(Q_{\text{nav}}^{i-1}, \text{dim} = 0), \text{dim} = 1), \\ Q_{\text{nav}}^i &= \text{CrossAttn}(\hat{Q}_{\text{nav}}^{i-1}, E_{\text{enc}}, E_{\text{enc}}). \end{aligned} \quad (4)$$

SelfAttn, CrossAttn denote multi-head self-attention and cross-attention operations, respectively. Given the decoder’s final output Q_{dec} , two MLP heads are applied to produce the CBV-centered multimodal trajectories $\mathcal{T} \in \mathbb{R}^{N_{\text{ref}} \times N_{\text{lon}} \times T \times 6}$ and their corresponding confidence scores $\mathcal{S} \in \mathbb{R}^{N_{\text{ref}} \times N_{\text{lon}}}$:

$$\mathcal{T} = \text{MLP}(Q_{\text{dec}}), \quad \mathcal{S} = \text{MLP}(Q_{\text{dec}}), \quad (5)$$

where T is the prediction horizon, and each trajectory point τ_t^i encodes $[p_x, p_y, \cos \theta, \sin \theta, v_x, v_y]$.

4 Methodology

Leveraging the trajectory generation model described in Section 3.2, realistic and multimodal trajectories can be generated across diverse scenarios. However, the open-loop training paradigm leaves the policy vulnerable to covariate shift, a distribution mismatch between expert states observed during training and those encountered at deployment, even equipped with techniques such as contrastive learning [54, 55] or data augmentation [53]. To mitigate this issue, we propose *RIFT*, a simple yet effective closed-loop RL fine-tuning strategy designed to enhance controllability and mitigate covariate shift while maintaining trajectory-level realism and multimodality. The following sections detail *RIFT*’s implementation within the dual-stage AV-centered simulation framework.

4.1 Critical Background Vehicle Identification

Following [1], we address the “curse of rarity” [56] by selectively intervening in a subset of critical background vehicles (CBVs) at key interaction moments, while retaining rule-based control for non-critical agents to reduce computational overhead.

To facilitate meaningful interactions between the AV and surrounding BVs, we adopt the principle of decoupling *route-level interaction* from *behavior-level realism*, as inspired by [57]. As illustrated in Figure 2, we estimate the route-level interaction probability between the AV’s predefined global route and the candidate routes of other BVs. The vehicle with the highest interaction probability is selected as the CBV, and its route is then synthesized based on the predicted conflict point to support further AV-centered closed-loop simulation. Further identification details are provided in Appendix B.2.

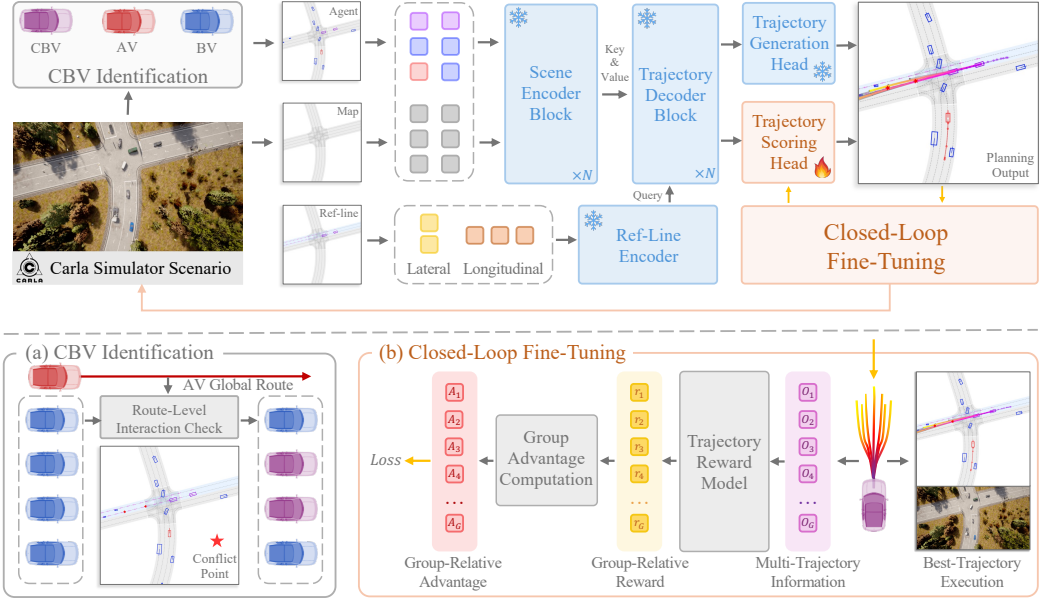


Figure 2: **Overview of the RIFT**: The upper section illustrates the overall architecture of *RIFT*. To enhance controllability, only the trajectory scoring head is fine-tuned, with the rest of the pre-trained network kept frozen to preserve trajectory-level realism. (a) The CBV identification mechanism introduces route-level interactions between the AV and CBVs. (b) Closed-loop fine-tuning improves user-aligned controllability and mitigates covariate shift.

4.2 Closed-Loop RL Fine-Tuning

For the identified CBVs, we replace rule-based control with the IL pre-trained trajectory generation model (Section 3.2), which generates $N_{\text{ref}} \times N_{\text{lon}}$ candidate trajectories per CBV. The highest-scoring trajectory is selected for closed-loop execution. However, due to the covariate shift between open-loop training and closed-loop deployment, this approach often accumulates errors over time, resulting in unrealistic long-term behavior. To address this issue, prior work has explored RL [58, 59] and hybrid IL-RL approaches [21, 22] for closed-loop fine-tuning. However, these methods typically compute the loss only on the executed action or the best trajectory, overlooking the remaining candidates and neglecting the inherently multimodal nature of real-world driving behaviors. Motivated by the success of GRPO [20] in large language models fine-tuning, we propose to treat all the candidate trajectories $\mathcal{T} = \{\tau_i\}_{i=1}^{N_{\text{ref}} \times N_{\text{lon}}}$ as a group output. We then compute the corresponding trajectory-level group-relative reward $\mathcal{R} = \{r_i\}_{i=1}^{N_{\text{ref}} \times N_{\text{lon}}}$ and the group-relative advantage $\mathcal{A} = \{\hat{A}_i\}_{i=1}^G$ as follows:

$$r_i = \sum_{t=0}^T \gamma^t [\text{StateWiseRM}(\tau_i^t)], \quad \hat{A}_i = \frac{r_i - \text{mean}(\mathcal{R})}{\text{std}(\mathcal{R})}, \quad \forall i = 1, \dots, G \quad (6)$$

where $G = N_{\text{ref}} \times N_{\text{lon}}$, and StateWiseRM is the user-defined state-wise reward model. With the group relative advantage \mathcal{A} , we derive the GRPO objective in our framework as:

$$\begin{aligned} \mathcal{J}_{\text{GRPO}}(\theta) &= \mathbb{E}_{[\{\tau_i\}_{i=1}^G \sim \pi_{\theta_{\text{old}}}(s)]} \\ &\quad \frac{1}{G} \sum_{i=1}^G \left\{ \min \left[\frac{\pi_{\theta}(\tau_i|s)}{\pi_{\theta_{\text{old}}}(\tau_i|s)} \hat{A}_i, \text{clip} \left(\frac{\pi_{\theta}(\tau_i|s)}{\pi_{\theta_{\text{old}}}(\tau_i|s)}, 1 - \epsilon, 1 + \epsilon \right) \hat{A}_i \right] - \beta \mathbb{D}_{\text{KL}} [\pi_{\theta} || \pi_{\text{ref}}] \right\}, \end{aligned} \quad (7)$$

where π_{θ} is the current trajectory generation model, π_{ref} is the reference policy model, ϵ and β are hyper-parameters, and $\rho_i(\theta) = \pi_{\theta}(\tau_i|s)/\pi_{\theta_{\text{old}}}(\tau_i|s)$ is the trajectory-level importance sampling ratio.

By leveraging IL pre-training to capture trajectory-level realism and multimodality, our closed-loop RL fine-tuning serves as an alignment mechanism that bridges the gap between user preferences and real-world data distributions, while preserving trajectory-level realism and multimodality. Building on this foundation, we remove the KL regularization term used in the original GRPO formulation, as

the IL pre-trained distribution may significantly diverge from the user-preferred output. In such cases, enforcing constraints via KL divergence is unnecessary and may hinder alignment.

Removing the KL regularization introduces instability during fine-tuning. PPO-Clip [58] addresses this by constraining updates through a clipped importance sampling ratio, effectively limiting policy shifts to a trust region. However, this mechanism is inadequate in our group-relative setting. The original clipping mechanism is designed for on-policy learning, where only the executed action is corrected. In contrast, we evaluate an entire set of trajectory candidates, where the trajectory-level importance ratio $\rho_i(\theta) = \pi_\theta(\tau_i|s)/\pi_{\theta_{\text{old}}}(\tau_i|s)$ can become arbitrarily large, especially when $\pi_\theta(\tau_i|s)$ dominates $\pi_{\theta_{\text{old}}}(\tau_i|s)$ and $\hat{A}_i < 0$, the resulting product $\rho_i(\theta)\hat{A}_i$ yields large negative values, leading to high variance and unstable updates. To stabilize fine-tuning while preserving alignment with user-defined preferences, we adopt the dual-clip mechanism from Dual-Clip PPO [60, 61], where a constant $c > 1$ acts as a lower bound on clipped negative advantages. The resulting *RIFT* objective is defined below (see Appendix A for theoretical analysis).

$$\begin{aligned} \mathcal{J}_{\text{RIFT}}(\theta) = & \mathbb{E}_{[\{\tau_i\}_{i=1}^G \sim \pi_{\theta_{\text{old}}}(s)]} \\ & \frac{1}{G} \sum_{i=1}^G \left\{ \max \left[\min \left[\frac{\pi_\theta(\tau_i|s)}{\pi_{\theta_{\text{old}}}(\tau_i|s)} \hat{A}_i, \text{clip} \left(\frac{\pi_\theta(\tau_i|s)}{\pi_{\theta_{\text{old}}}(\tau_i|s)}, 1 - \epsilon, 1 + \epsilon \right) \hat{A}_i \right], c\hat{A}_i \right] \right\}. \end{aligned} \quad (8)$$

5 Experiment

This section systematically investigates the following research questions: **Q1**: How do the realism and controllability of interactive scenarios generated by *RIFT* compare to the baselines? **Q2**: How can the generated scenarios be leveraged for downstream tasks in autonomous driving? **Q3**: What are the contributions of each component within *RIFT* to the overall performance, and how well is controllability preserved under different user-specified reward settings? We first present the experimental setup, including the environment, baseline methods, and evaluation metrics. We then analyze the results to address these research questions.

5.1 Experiment Setups

Under the dual-stage AV-centered simulation framework, we adopt Pluto [53] as our trajectory generation model, owing to its strong performance and publicly available implementation. To ensure fairness during pre-training, we directly utilize the IL pre-trained checkpoint released by Pluto, which was pre-trained on the nuPlan dataset [11]. This setup enables a focused investigation of closed-loop fine-tuning. We conduct simulations in CARLA [62], building upon the Bench2Drive [46] framework to support comprehensive AV-centered closed-loop simulation and evaluation. Additional details regarding implementation, framework design, training protocols, and evaluation settings are provided in Appendix B.

Baseline. To systematically evaluate the effectiveness of *RIFT* in closed-loop fine-tuning, we compare it against the following baselines (details are provided in Appendix B.5).

- **Pure RL/IL:** Methods trained purely with either RL or IL without fine-tuning, including *Pluto* [53], *FREA* [14], *FPPO-RS* [14], and *PPO* [14].
- **RLFT/SFT:** Methods that apply RL or supervised signals to fine-tune the pre-trained Pluto models, such as *PPO-Pluto* [58], *REINFORCE-Pluto* [59], *GRPO-Pluto* [20], and *SFT-Pluto*.
- **Hybrid:** Methods that integrate both RL and supervised signals during fine-tuning, including *RTR-Pluto* [21] and *RS-Pluto* [22].

All methods are fine-tuned on the same module—the trajectory scoring head of Pluto—to ensure fair comparisons and decouple trajectory-level realism from behavior-level reliability, as confirmed by the ablation studies in Section 5.4. Following the realism standards of the Sim Agent Challenge in WOSAC [34], we adopt a normal reward setting for all RL-based baselines, with the detailed configuration provided in Appendix B.6. Results under an aggressive reward configuration are also reported in Section 5.4.

Metrics. We extend the WOSAC evaluation framework [34], which evaluates behavior controllability and realism across three key categories—*motion*, *agent interactions*, and *map adherence*—to define our own set of evaluation metrics, as inspired by [63]. More details are provided in Appendix B.7.

Table 1: **Comparison in Controllability and Realism.** Metrics are evaluated under the PDM-Lite [69] AV setting across three random seeds, with the **best** and the **second-best** results highlighted accordingly.

Method	Type	Controllability					Realism		
		Infraction		Progress		Safety		Speed	
		ORR \downarrow	CPK \downarrow	RP \uparrow	2D-TTC \uparrow	ACT \uparrow	SW \uparrow	WD \downarrow	SW \uparrow
Pluto [53]	IL	0.24 \pm 0.15	5.06 \pm 2.69	564.14 \pm 114.41	2.50 \pm 1.48	2.44 \pm 1.39	0.88 \pm 0.01	5.81 \pm 0.06	0.90 \pm 0.01
PPO [14]	RL	9.17 \pm 2.39	13.95 \pm 2.34	409.51 \pm 30.38	2.59 \pm 1.60	2.52 \pm 1.57	0.95 \pm 0.01	4.45 \pm 0.15	0.89 \pm 0.02
FREA [14]	RL	9.01 \pm 2.09	30.42 \pm 5.28	292.81 \pm 68.54	2.71 \pm 1.40	2.67 \pm 1.41	0.93 \pm 0.01	5.10 \pm 0.14	0.93 \pm 0.01
FFPO-RS [14]	RL	8.60 \pm 0.25	21.39 \pm 3.23	356.79 \pm 26.19	2.55 \pm 1.69	2.53 \pm 1.68	0.87 \pm 0.01	5.80 \pm 0.11	0.80 \pm 0.03
SFT-Pluto	SFT	0.06 \pm 0.07	6.33 \pm 2.23	780.48 \pm 41.05	2.20 \pm 1.64	2.12 \pm 1.51	0.88 \pm 0.02	6.01 \pm 0.19	0.87 \pm 0.02
RS-Pluto [22]	SFT+RLFT	1.05 \pm 0.31	4.11 \pm 3.90	819.40 \pm 74.07	2.27 \pm 1.45	2.23 \pm 1.43	0.93 \pm 0.00	5.40 \pm 0.15	0.92 \pm 0.01
RTR-Pluto [21]	SFT+RLFT	0.08 \pm 0.09	6.98 \pm 2.59	481.60 \pm 70.19	2.55 \pm 1.60	2.47 \pm 1.51	0.85 \pm 0.00	6.24 \pm 0.16	0.81 \pm 0.03
PPO-Pluto	RLFT	0.07 \pm 0.13	6.89 \pm 3.19	683.57 \pm 38.12	2.66 \pm 1.50	2.60 \pm 1.43	0.95 \pm 0.01	4.96 \pm 0.31	0.90 \pm 0.02
REINFORCE-Pluto	RLFT	1.37 \pm 1.13	6.98 \pm 0.86	813.70 \pm 24.76	2.39 \pm 1.64	2.30 \pm 1.55	0.92 \pm 0.01	5.63 \pm 0.19	0.90 \pm 0.02
GRPO-Pluto	RLFT	0.10 \pm 0.08	7.24 \pm 4.04	892.65 \pm 65.27	2.65 \pm 1.44	2.61 \pm 1.48	0.94 \pm 0.04	4.96 \pm 0.89	0.96 \pm 0.00
RIFT-Pluto (ours)	RLFT	0.36 \pm 0.20	6.83 \pm 2.62	995.33 \pm 84.62	2.74 \pm 1.30	2.71 \pm 1.32	0.97 \pm 0.01	4.46 \pm 0.43	0.93 \pm 0.01

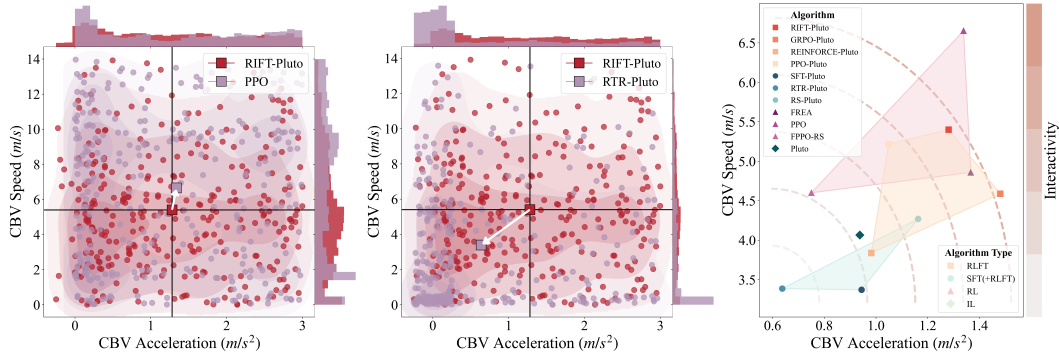


Figure 3: **Speed and Acceleration Distribution.** RL-based methods produce interactive but often unnatural behaviors, while supervised methods typically lead to conservative behavior. In contrast, *RIFT* achieves higher interactivity, reflected by increased average speed and acceleration, and more realistic behavior from the distributional perspective, avoiding unnecessary hesitation while keeping safe interactions.

- **Controllability:** We measure infractions using Scenario Collision Per Kilometer (CPK) and Off-Road Rate (ORR)[41, 42], evaluate driving progress via Route Progress (RP), and assess driving safety with safety-critical metrics such as 2D-TTC[64] and ACT [65].
- **Realism:** Quantifying realism in traffic scenarios remains a challenging problem. Inspired by prior work that evaluates realism from a distributional perspective [21, 34, 63]. We use the Shapiro–Wilk test (SW) [66, 67] to assess the normality of speed and acceleration, and Wasserstein Distance (WD) [68] to measure deviation from the target speed in the CARLA [62].

5.2 Realistic and Controllable Traffic Scenario Generation (Q1)

Main Results. To address **Q1**, we evaluate the controllability and realism of the generated scenarios across different CBV methods, with results summarized in Table 1. *RIFT* consistently outperforms all baselines in both aspects across most settings. While supervised learning methods achieve slightly lower infraction rates, this improvement is primarily due to their inherently conservative behavior, derived from the expert PDM-Lite [69], which prioritizes safety by avoiding risky maneuvers.

This conservative tendency is further highlighted in Figure 3, where supervised policies exhibit significantly lower speed and acceleration profiles. In contrast, *RIFT* strikes a more favorable balance between safety and interactivity. It achieves superior safety performance, as reflected by higher 2D-TTC and ACT scores, while avoiding the overly cautious behaviors typical of supervised approaches. As shown in Figure 3, *RIFT* demonstrates higher average speed and acceleration, indicating more interactive behavior, while maintaining realistic motion profiles.

Qualitative Results. To further demonstrate the effectiveness of *RIFT*, we present simulation results across a range of traffic scenarios under diverse conditions, including varying weather (e.g., rain and fog) and traffic scenarios (e.g., merging and crossing), as illustrated in Figure 4. These results demonstrate the robustness and generalizability of *RIFT* in challenging environments. In addition,

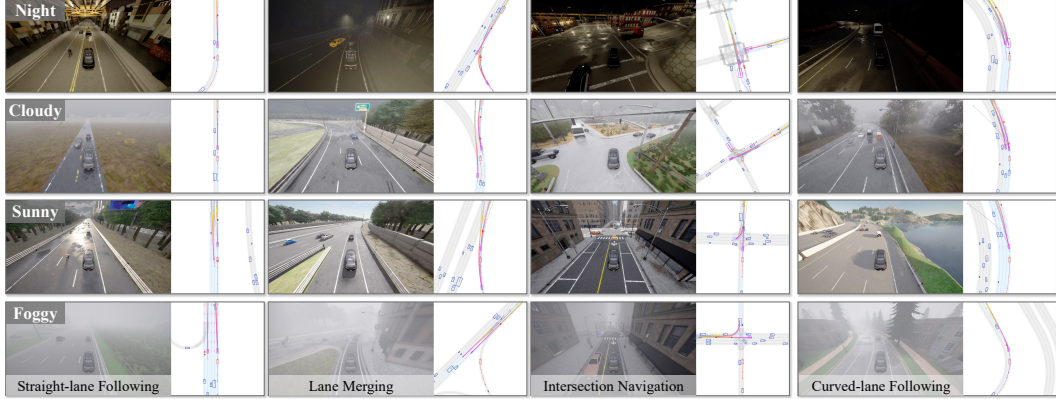


Figure 4: Qualitative examples illustrating the robustness of *RIFT* across diverse AV-centered traffic scenarios. CBV is marked in purple, AV (PDM-Lite) is in red, and BVs are in blue.

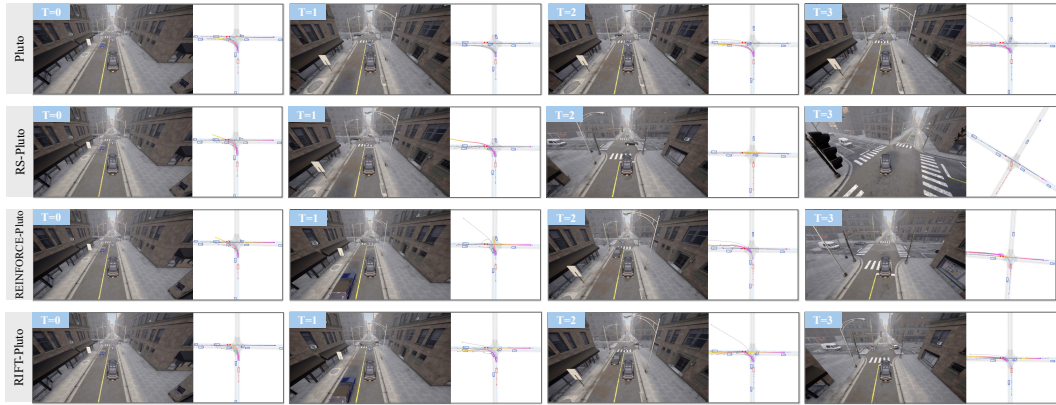


Figure 5: Temporal comparisons illustrating *RIFT*'s superior performance over other baselines under AV-centered closed-loop simulation. CBV is marked in purple, AV (PDM-Lite) is in red, and BVs are in blue.

we compare closed-loop simulations against representative baselines, as shown in Figure 5. Baseline methods often suffer from trajectory instability or poor-quality generation in closed-loop settings. In contrast, *RIFT* consistently generates smooth, high-quality trajectories with better temporal consistency. Additional qualitative results are provided in Appendix D.3.

5.3 Realistic Traffic Scenarios for Closed-Loop AV Evaluation (Q2)

In addressing **Q2**, we investigate the integration of *RIFT* into downstream tasks, specifically in the closed-loop AV evaluation. Building on the closed-loop evaluation framework [46, 70] in CARLA, we replace its hand-crafted scenarios with traffic flows generated by various CBV methods while retaining the same global route settings. To ensure fair and consistent evaluation, we adopt the standard AV evaluation metrics and introduce a new metric, Blocked Rate (BR), to measure situations where CBVs obstruct the AV. We evaluate two publicly available AV algorithms: the rule-based PDM-Lite [69] and the learning-based PlantT [71]. The results, presented in Table 2, demonstrate that under the *RIFT*-generated scenarios, AVs achieve near-optimal Driving Score (DS), Route Completion (RC), and Infraction Score (IS), along with the lowest BR. These findings highlight *RIFT*'s effectiveness in minimizing blocking while maintaining realism and interactivity, underscoring its superiority in closed-loop AV evaluation. Further details are available in Appendix C.

5.4 Ablation Study (Q3)

In exploring the design choices within *RIFT*, we conduct a series of ablation studies focusing on three key aspects: the choice of policy optimization clip (Dual-Clip vs. PPO-Clip), the fine-tuning module (Trajectory Scoring Head vs. All Head), and the reward design (Normal vs. Aggressive). All experiments are conducted under consistent settings, and results are summarized in Table 3.

Table 2: **Comparison of AV Evaluation across CBV Methods.** Each metric is evaluated across three random seeds, with the **best** and the **second-best** results highlighted accordingly.

Method	PDM-Lite [69]				PlanT [71]			
	DS \uparrow	RC \uparrow	IS \uparrow	BR \downarrow	DS \uparrow	RC \uparrow	IS \uparrow	BR \downarrow
Pluto [53]	77.84 \pm 2.20	81.84 \pm 2.20	0.96 \pm 0.00	23.33 \pm 5.77	42.52 \pm 4.72	52.53 \pm 5.29	0.79 \pm 0.01	46.67 \pm 15.28
PPO[14]	76.26 \pm 0.12	76.26 \pm 0.12	1.00 \pm 0.00	30.00 \pm 0.00	36.39 \pm 1.11	58.30 \pm 3.41	0.66 \pm 0.05	43.33 \pm 11.55
FREA[14]	83.53 \pm 0.13	83.53 \pm 0.13	1.00 \pm 0.00	20.00 \pm 0.00	39.61 \pm 1.34	53.82 \pm 2.20	0.73 \pm 0.01	56.67 \pm 5.77
FPPPO-RS[14]	83.52 \pm 0.09	83.52 \pm 0.09	1.00 \pm 0.00	20.00 \pm 0.00	38.85 \pm 4.91	52.27 \pm 5.38	0.66 \pm 0.07	50.00 \pm 10.00
SFT-Pluto	86.09 \pm 2.04	90.16 \pm 1.82	0.97 \pm 0.03	13.33 \pm 5.77	39.41 \pm 4.97	57.90 \pm 3.72	0.70 \pm 0.06	50.00 \pm 0.00
RS-Pluto [22]	89.32 \pm 1.41	89.32 \pm 1.41	1.00 \pm 0.00	13.33 \pm 5.77	42.05 \pm 4.08	59.58 \pm 3.27	0.66 \pm 0.02	50.00 \pm 0.00
RTR-Pluto [21]	87.64 \pm 1.56	91.64 \pm 1.56	0.96 \pm 0.00	10.00 \pm 0.00	40.08 \pm 2.38	55.87 \pm 1.71	0.69 \pm 0.04	50.00 \pm 0.00
PPO-Pluto	85.63 \pm 2.02	89.63 \pm 2.02	0.96 \pm 0.00	16.67 \pm 5.77	41.86 \pm 2.78	59.82 \pm 2.90	0.66 \pm 0.04	43.33 \pm 5.77
REINFORCE-Pluto	92.17 \pm 3.45	92.17 \pm 3.45	1.00 \pm 0.00	10.00 \pm 10.00	45.25 \pm 1.75	63.74 \pm 5.91	0.67 \pm 0.05	43.33 \pm 5.77
GRPO-Pluto	89.86 \pm 2.10	91.19 \pm 3.46	0.99 \pm 0.02	6.67 \pm 5.77	47.24 \pm 5.67	61.88 \pm 0.71	0.75 \pm 0.07	33.33 \pm 5.77
RIFT-Pluto (ours)	94.78 \pm 1.37	94.78 \pm 1.37	1.00 \pm 0.00	0.00 \pm 0.00	44.28 \pm 3.15	61.94 \pm 5.08	0.64 \pm 0.02	40.00 \pm 10.00

Table 3: **Ablation study on RIFT.** Evaluation under PDM-Lite [69] AV setting with three random seeds.

Method	Controllability					Realism		
	Infraction		Progress		Safety	Speed		Acceleration
	ORR \downarrow	CPK \downarrow	RP \uparrow	2D-TTC \uparrow	ACT \uparrow	SW \uparrow	WD \downarrow	SW \uparrow
w/ Aggressive	0.91 $\textcolor{blue}{(+0.55)}$	8.41 $\textcolor{blue}{(+1.58)}$	1053.76 $\textcolor{blue}{(+58.43)}$	2.93 $\textcolor{blue}{(+0.19)}$	2.88 $\textcolor{blue}{(+0.17)}$	0.97 $\textcolor{blue}{(+0.00)}$	3.89 $\textcolor{blue}{(-0.57)}$	0.94 $\textcolor{blue}{(+0.01)}$
w/ All-head	0.43 $\textcolor{blue}{(+0.07)}$	7.84 $\textcolor{blue}{(+1.01)}$	827.12 $\textcolor{blue}{(168.21)}$	2.83 $\textcolor{blue}{(+0.09)}$	2.76 $\textcolor{blue}{(+0.05)}$	0.96 $\textcolor{blue}{(-0.01)}$	4.70 $\textcolor{blue}{(+0.24)}$	0.94 $\textcolor{blue}{(+0.01)}$
w/ PPO-Clip	0.04 $\textcolor{blue}{(-0.32)}$	2.03 $\textcolor{blue}{(-4.80)}$	655.39 $\textcolor{blue}{(-339.94)}$	2.57 $\textcolor{blue}{(-0.17)}$	2.54 $\textcolor{blue}{(-0.17)}$	0.91 $\textcolor{blue}{(-0.06)}$	5.92 $\textcolor{blue}{(+1.46)}$	0.94 $\textcolor{blue}{(+0.01)}$
RIFT-Pluto (ours)	0.36	6.83	995.33	2.74	2.71	0.97	4.46	0.93

Dual-Clip vs. PPO-Clip. We first evaluate the effect of the dual-clip mechanism by replacing it with the standard PPO-Clip (*w/ PPO-Clip*). This variant leads to more conservative and less realistic behaviors, as evidenced by reduced Progress and degraded Speed Realism metrics.

Trajectory Scoring Head vs. All Head. Next, we examine the impact of the fine-tuning module on performance by comparing *RIFT* fine-tuned using only the trajectory scoring head with a variant fine-tuned on all heads (*w/ All Head*). The latter results in a slight drop across Realism, Progress, and Infraction metrics, likely due to the disruption of trajectory-level realism captured during pre-training.

Normal vs. Aggressive. Finally, we explore the effect of different reward preferences on controllability by adopting a more aggressive reward focused on driving efficiency (*w/ Aggressive*). This variant improves Progress and Speed Realism but increases Infractions, reflecting the intended trade-off and confirming that *RIFT* allows flexible reward design while preserving user controllability. Additional qualitative results regarding controllability are presented in Appendix D.1.

6 Conclusion

In this work, we propose a dual-stage AV-centered simulation framework that conducts open-loop IL pre-training in a data-driven simulator to capture trajectory-level realism and multimodality, followed by closed-loop RL fine-tuning in a physics-based simulator to address the covariate shift problem and enhance controllability. During fine-tuning, we introduce *RIFT*, a simple yet effective closed-loop RL fine-tuning strategy that preserves the trajectory-level multimodality through a GRPO-style group-relative advantage formulation and enhances both controllability and training stability by replacing KL regularization with the dual-clip mechanism. Extensive experiments demonstrate that *RIFT* generates high-quality traffic scenarios that are both realistic and controllable, offering a reliable simulation environment for evaluating AV performance in diverse and interactive scenarios, thus bridging the gap between scenario generation and closed-loop AV evaluation.

Limitations and Future Work. Currently, *RIFT* adopts a simple state-wise reward model, StateWiseRM, as detailed in Appendix B.6, to evaluate each trajectory point without forward simulation. This may result in inaccurate trajectory-level reward estimations over time, potentially affecting closed-loop RL fine-tuning performance (further discussed in Appendix D.2). Additionally, the current implementation of our traffic simulation framework supports only AV methods with fully observable, vectorized scene representations. Extending this framework to support end-to-end closed-loop training and evaluation remains a promising direction for future research.

References

- [1] Shuo Feng, Haowei Sun, Xintao Yan, Haojie Zhu, Zhengxia Zou, Shengyin Shen, and Henry X Liu. Dense reinforcement learning for safety validation of autonomous vehicles. *Nature*, 615(7953):620–627, 2023. [1](#) [4](#)
- [2] Wenhao Ding, Chejian Xu, Mansur Arief, Haohong Lin, Bo Li, and Ding Zhao. A survey on safety-critical driving scenario generation—a methodological perspective. *IEEE Transactions on Intelligent Transportation Systems*, 2023. [1](#)
- [3] Zhejun Zhang, Alexander Liniger, Dengxin Dai, Fisher Yu, and Luc Van Gool. Trafficbots: Towards world models for autonomous driving simulation and motion prediction. In *2023 IEEE International Conference on Robotics and Automation (ICRA)*, pages 1522–1529. IEEE, 2023. [1](#)
- [4] Reza Mahjourian, Rongbing Mu, Valerii Likhosherstov, Paul Mougin, Xiukun Huang, Joao Messias, and Shimon Whiteson. Unigen: Unified modeling of initial agent states and trajectories for generating autonomous driving scenarios. In *2024 IEEE International Conference on Robotics and Automation (ICRA)*, pages 16367–16373. IEEE, 2024. [1](#)
- [5] Shuhan Tan, Kelvin Wong, Shenlong Wang, Sivabalan Manivasagam, Mengye Ren, and Raquel Urtasun. Scenegen: Learning to generate realistic traffic scenes. In *Proceedings of the IEEE/CVF Conference on Computer Vision and Pattern Recognition*, pages 892–901, 2021. [1](#)
- [6] Lan Feng, Quanyi Li, Zhenghao Peng, Shuhan Tan, and Bolei Zhou. Trafficgen: Learning to generate diverse and realistic traffic scenarios. In *2023 IEEE International Conference on Robotics and Automation (ICRA)*, pages 3567–3575. IEEE, 2023.
- [7] Jiawei Zhang, Chejian Xu, and Bo Li. Chatscene: Knowledge-enabled safety-critical scenario generation for autonomous vehicles. In *Proceedings of the IEEE/CVF Conference on Computer Vision and Pattern Recognition*, pages 15459–15469, 2024. [1](#)
- [8] Jiquan Ngiam, Benjamin Caine, Vijay Vasudevan, Zhengdong Zhang, Hao-Tien Lewis Chiang, Jeffrey Ling, Rebecca Roelofs, Alex Bewley, Chenxi Liu, Ashish Venugopal, et al. Scene transformer: A unified architecture for predicting multiple agent trajectories. *arXiv preprint arXiv:2106.08417*, 2021. [1](#)
- [9] Qiao Sun, Xin Huang, Brian C Williams, and Hang Zhao. Intersim: Interactive traffic simulation via explicit relation modeling. In *2022 IEEE/RSJ International Conference on Intelligent Robots and Systems (IROS)*, pages 11416–11423. IEEE, 2022. [1](#)
- [10] Cole Gulino, Justin Fu, Wenjie Luo, George Tucker, Eli Bronstein, Yiren Lu, Jean Harb, Xinlei Pan, Yan Wang, Xiangyu Chen, et al. Waymax: An accelerated, data-driven simulator for large-scale autonomous driving research. *Advances in Neural Information Processing Systems*, 36:7730–7742, 2023. [1](#) [3](#)
- [11] Holger Caesar, Juraj Kabzan, Kok Seang Tan, Whye Kit Fong, Eric Wolff, Alex Lang, Luke Fletcher, Oscar Beijbom, and Sammy Omari. nuplan: A closed-loop ml-based planning benchmark for autonomous vehicles. *arXiv preprint arXiv:2106.11810*, 2021. [1](#) [3](#) [6](#) [19](#)
- [12] Wenhao Ding, Baiming Chen, Bo Li, Kim Ji Eun, and Ding Zhao. Multimodal safety-critical scenarios generation for decision-making algorithms evaluation. *IEEE Robotics and Automation Letters*, 6(2):1551–1558, 2021. [2](#)
- [13] Niklas Hanselmann, Katrin Renz, Kashyap Chitta, Apratim Bhattacharyya, and Andreas Geiger. King: Generating safety-critical driving scenarios for robust imitation via kinematics gradients. In *European Conference on Computer Vision*, pages 335–352. Springer, 2022.
- [14] Keyu Chen, Yuheng Lei, Hao Cheng, Haoran Wu, Wenchoa Sun, and Sifa Zheng. FREA: Feasibility-guided generation of safety-critical scenarios with reasonable adversariality. In *8th Annual Conference on Robot Learning*, 2024. [6](#) [7](#) [9](#) [19](#) [20](#) [24](#)
- [15] Linrui Zhang, Zhenghao Peng, Quanyi Li, and Bolei Zhou. Cat: Closed-loop adversarial training for safe end-to-end driving. In *7th Annual Conference on Robot Learning*, 2023. [2](#)
- [16] Błażej Osiński, Piotr Miłoś, Adam Jakubowski, Paweł Zięcina, Michał Martyniak, Christopher Galias, Antonia Breuer, Silviu Homoceanu, and Henryk Michalewski. Carla real traffic scenarios—novel training ground and benchmark for autonomous driving. *arXiv preprint arXiv:2012.11329*, 2020. [2](#)
- [17] Quanyi Li, Zhenghao Peng, Lan Feng, Zhizheng Liu, Chenda Duan, Wenjie Mo, and Bolei Zhou. Scenarionet: Open-source platform for large-scale traffic scenario simulation and modeling. *Advances in Neural Information Processing Systems*, 2023. [2](#)

[18] Rafael Rafailov, Archit Sharma, Eric Mitchell, Christopher D Manning, Stefano Ermon, and Chelsea Finn. Direct preference optimization: Your language model is secretly a reward model. *Advances in Neural Information Processing Systems*, 36:53728–53741, 2023. 2

[19] Qiying Yu, Zheng Zhang, Ruofei Zhu, Yufeng Yuan, Xiaochen Zuo, Yu Yue, Tiantian Fan, Gaohong Liu, Lingjun Liu, Xin Liu, et al. Dapo: An open-source llm reinforcement learning system at scale. *arXiv preprint arXiv:2503.14476*, 2025.

[20] Zhihong Shao, Peiyi Wang, Qihao Zhu, Runxin Xu, Junxiao Song, Xiao Bi, Haowei Zhang, Mingchuan Zhang, YK Li, Y Wu, et al. Deepseekmath: Pushing the limits of mathematical reasoning in open language models. *arXiv preprint arXiv:2402.03300*, 2024. 2, 5, 6, 16, 20

[21] Chris Zhang, James Tu, Lunjun Zhang, Kelvin Wong, Simon Suo, and Raquel Urtasun. Learning realistic traffic agents in closed-loop. In *7th Annual Conference on Robot Learning*, 2023. 2, 3, 5, 6, 7, 9, 20, 24

[22] Zhenghao Peng, Wenjie Luo, Yiren Lu, Tianyi Shen, Cole Gulino, Ari Seff, and Justin Fu. Improving agent behaviors with rl fine-tuning for autonomous driving. In *European Conference on Computer Vision*, pages 165–181. Springer, 2024. 2, 3, 5, 6, 7, 9, 20, 24

[23] Simon Suo, Sebastian Regalado, Sergio Casas, and Raquel Urtasun. Trafficsim: Learning to simulate realistic multi-agent behaviors. In *Proceedings of the IEEE/CVF Conference on Computer Vision and Pattern Recognition*, pages 10400–10409, 2021. 3

[24] Davis Rempe, Jonah Philion, Leonidas J Guibas, Sanja Fidler, and Or Litany. Generating useful accident-prone driving scenarios via a learned traffic prior. In *Proceedings of the IEEE/CVF Conference on Computer Vision and Pattern Recognition*, pages 17305–17315, 2022.

[25] Danfei Xu, Yuxiao Chen, Boris Ivanovic, and Marco Pavone. Bits: Bi-level imitation for traffic simulation. In *2023 IEEE International Conference on Robotics and Automation (ICRA)*, pages 2929–2936. IEEE, 2023. 3

[26] Chiyu Max Jiang, Yijing Bai, Andre Cornman, Christopher Davis, Xiukun Huang, Hong Jeon, Sakshum Kulshrestha, John Wheatley Lambert, Shuangyu Li, Xuanyu Zhou, Carlos Fuentes, Chang Yuan, Mingxing Tan, Yin Zhou, and Dragomir Anguelov. Scenediffuser: Efficient and controllable driving simulation initialization and rollout. In *The Thirty-eighth Annual Conference on Neural Information Processing Systems*, 2024. 3

[27] Kashyap Chitta, Daniel Dauner, and Andreas Geiger. Sledge: Synthesizing driving environments with generative models and rule-based traffic. In *European Conference on Computer Vision*, pages 57–74. Springer, 2024.

[28] Yunsong Zhou, Naisheng Ye, William Ljungbergh, Tianyu Li, Jiazhi Yang, Zetong Yang, Hongzi Zhu, Christoffer Petersson, and Hongyang Li. Decoupled diffusion sparks adaptive scene generation. *arXiv preprint arXiv:2504.10485*, 2025. 3

[29] Wei Wu, Xiaoxin Feng, Ziyan Gao, and Yuheng Kan. Smart: Scalable multi-agent real-time motion generation via next-token prediction. *Advances in Neural Information Processing Systems*, 37:114048–114071, 2024. 3

[30] Yihan Hu, Siqi Chai, Zhenning Yang, Jingyu Qian, Kun Li, Wenxin Shao, Haichao Zhang, Wei Xu, and Qiang Liu. Solving motion planning tasks with a scalable generative model. In *European Conference on Computer Vision*, pages 386–404. Springer, 2024. 3

[31] Jonah Philion, Xue Bin Peng, and Sanja Fidler. Trajeglish: Traffic modeling as next-token prediction. In *The Twelfth International Conference on Learning Representations*, 2023. 3

[32] Ari Seff, Brian Cera, Dian Chen, Mason Ng, Aurick Zhou, Nigamaa Nayakanti, Khaled S Refaat, Rami Al-Rfou, and Benjamin Sapp. Motionlm: Multi-agent motion forecasting as language modeling. In *Proceedings of the IEEE/CVF International Conference on Computer Vision*, pages 8579–8590, 2023. 3

[33] Daniel Dauner, Marcel Hallgarten, Tianyu Li, Xinshuo Weng, Zhiyu Huang, Zetong Yang, Hongyang Li, Igor Gilitschenski, Boris Ivanovic, Marco Pavone, et al. Navsim: Data-driven non-reactive autonomous vehicle simulation and benchmarking. *Advances in Neural Information Processing Systems*, 37:28706–28719, 2024. 3

[34] Nico Montali, John Lambert, Paul Mougin, Alex Kuefler, Nicholas Rhinehart, Michelle Li, Cole Gulino, Tristan Emrich, Zoey Yang, Shimon Whiteson, et al. The waymo open sim agents challenge. *Advances in Neural Information Processing Systems*, 36:59151–59171, 2023. 3, 6, 7, 21

[35] Ziyuan Zhong, Davis Rempe, Danfei Xu, Yuxiao Chen, Sushant Veer, Tong Che, Baishakhi Ray, and Marco Pavone. Guided conditional diffusion for controllable traffic simulation. In *2023 IEEE international conference on robotics and automation (ICRA)*, pages 3560–3566. IEEE, 2023. 3

[36] Chiyu Jiang, Andre Cornman, Cheolho Park, Benjamin Sapp, Yin Zhou, Dragomir Anguelov, et al. Motiondiffuser: Controllable multi-agent motion prediction using diffusion. In *Proceedings of the IEEE/CVF conference on computer vision and pattern recognition*, pages 9644–9653, 2023. 3

[37] Ziyuan Zhong, Davis Rempe, Yuxiao Chen, Boris Ivanovic, Yulong Cao, Danfei Xu, Marco Pavone, and Baishakhi Ray. Language-guided traffic simulation via scene-level diffusion. *arXiv preprint arXiv:2306.06344*, 2023. 3

[38] Shuhan Tan, Boris Ivanovic, Xinshuo Weng, Marco Pavone, and Philipp Krahenbuehl. Language conditioned traffic generation. *arXiv preprint arXiv:2307.07947*, 2023. 3

[39] Shuhan Tan, Boris Ivanovic, Yuxiao Chen, Boyi Li, Xinshuo Weng, Yulong Cao, Philipp Krähenbühl, and Marco Pavone. Promptable closed-loop traffic simulation. In *8th Annual Conference on Robot Learning*, 2024. 3

[40] Jack Lu, Kelvin Wong, Chris Zhang, Simon Suo, and Raquel Urtasun. Scenecontrol: Diffusion for controllable traffic scene generation. In *2024 IEEE International Conference on Robotics and Automation (ICRA)*, pages 16908–16914. IEEE, 2024. 3

[41] Wenhao Ding, Yulong Cao, Ding Zhao, Chaowei Xiao, and Marco Pavone. Realgen: Retrieval augmented generation for controllable traffic scenarios. In *European Conference on Computer Vision*, pages 93–110. Springer, 2024. 3, 7

[42] Haohong Lin, Xin Huang, Tung Phan-Minh, David S Hayden, Huan Zhang, Ding Zhao, Siddhartha Srinivasa, Eric M Wolff, and Hongge Chen. Causal composition diffusion model for closed-loop traffic generation. *arXiv preprint arXiv:2412.17920*, 2024. 3, 7, 21

[43] Yiren Lu, Justin Fu, George Tucker, Xinlei Pan, Eli Bronstein, Rebecca Roelofs, Benjamin Sapp, Brandy White, Aleksandra Faust, Shimon Whiteson, et al. Imitation is not enough: Robustifying imitation with reinforcement learning for challenging driving scenarios. In *2023 IEEE/RSJ International Conference on Intelligent Robots and Systems (IROS)*, pages 7553–7560. IEEE, 2023. 3

[44] Zhejun Zhang, Peter Karkus, Maximilian Igl, Wenhao Ding, Yuxiao Chen, Boris Ivanovic, and Marco Pavone. Closed-loop supervised fine-tuning of tokenized traffic models. In *Proceedings of the IEEE Conference on Computer Vision and Pattern Recognition (CVPR)*, 2025. 3

[45] Yulong Cao, Boris Ivanovic, Chaowei Xiao, and Marco Pavone. Reinforcement learning with human feedback for realistic traffic simulation. In *2024 IEEE International Conference on Robotics and Automation (ICRA)*, pages 14428–14434. IEEE, 2024. 3

[46] Xiaosong Jia, Zhenjie Yang, Qifeng Li, Zhiyuan Zhang, and Junchi Yan. Bench2drive: Towards multi-ability benchmarking of closed-loop end-to-end autonomous driving. *arXiv preprint arXiv:2406.03877*, 2024. 3, 6, 8, 18

[47] Chejian Xu, Wenhao Ding, Weijie Lyu, Zuxin Liu, Shuai Wang, Yihan He, Hanjiang Hu, Ding Zhao, and Bo Li. Safebench: A benchmarking platform for safety evaluation of autonomous vehicles. *Advances in Neural Information Processing Systems*, 35:25667–25682, 2022. 3

[48] Yinan Zheng, Ruiming Liang, Kexin ZHENG, Jinliang Zheng, Liyuan Mao, Jianxiong Li, Weihao Gu, Rui Ai, Shengbo Eben Li, Xianyuan Zhan, and Jingjing Liu. Diffusion-based planning for autonomous driving with flexible guidance. In *The Thirteenth International Conference on Learning Representations*, 2025. 3

[49] Zhiyu Huang, Haochen Liu, and Chen Lv. Gameformer: Game-theoretic modeling and learning of transformer-based interactive prediction and planning for autonomous driving. In *Proceedings of the IEEE/CVF International Conference on Computer Vision (ICCV)*, pages 3903–3913, October 2023.

[50] Yihan Hu, Jiazheng Yang, Li Chen, Keyu Li, Chonghao Sima, Xizhou Zhu, Siqi Chai, Senyao Du, Tianwei Lin, Wenhui Wang, Lewei Lu, Xiaosong Jia, Qiang Liu, Jifeng Dai, Yu Qiao, and Hongyang Li. Planning-oriented autonomous driving. In *Proceedings of the IEEE/CVF Conference on Computer Vision and Pattern Recognition*, 2023.

[51] Bo Jiang, Shaoyu Chen, Qing Xu, Bencheng Liao, Jiajie Chen, Helong Zhou, Qian Zhang, Wenyu Liu, Chang Huang, and Xinggang Wang. Vad: Vectorized scene representation for efficient autonomous driving. *ICCV*, 2023.

[52] Wenchao Sun, Xuewu Lin, Yining Shi, Chuang Zhang, Haoran Wu, and Sifa Zheng. Sparsedrive: End-to-end autonomous driving via sparse scene representation. *arXiv preprint arXiv:2405.19620*, 2024. 3

[53] Jie Cheng, Yingbing Chen, and Qifeng Chen. Pluto: Pushing the limit of imitation learning-based planning for autonomous driving. *arXiv preprint arXiv:2404.14327*, 2024. 3, 4, 6, 7, 9, 19, 21, 24

[54] Marah Halawa, Olaf Hellwich, and Pia Bideau. Action-based contrastive learning for trajectory prediction. In *European conference on computer vision*, pages 143–159. Springer, 2022. 4

[55] Yuning Wang, Pu Zhang, Lei Bai, and Jianru Xue. Fend: A future enhanced distribution-aware contrastive learning framework for long-tail trajectory prediction. In *Proceedings of the IEEE/CVF conference on computer vision and pattern recognition*, pages 1400–1409, 2023. 4

[56] Henry X Liu and Shuo Feng. Curse of rarity for autonomous vehicles. *nature communications*, 15(1):4808, 2024. 4

[57] Simon Suo, Kelvin Wong, Justin Xu, James Tu, Alexander Cui, Sergio Casas, and Raquel Urtasun. Mixsim: A hierarchical framework for mixed reality traffic simulation. In *Proceedings of the IEEE/CVF Conference on Computer Vision and Pattern Recognition*, pages 9622–9631, 2023. 4

[58] John Schulman, Filip Wolski, Prafulla Dhariwal, Alec Radford, and Oleg Klimov. Proximal policy optimization algorithms. *arXiv preprint arXiv:1707.06347*, 2017. 5, 6, 20

[59] Richard S Sutton, David McAllester, Satinder Singh, and Yishay Mansour. Policy gradient methods for reinforcement learning with function approximation. *Advances in neural information processing systems*, 12, 1999. 5, 6, 20

[60] Deheng Ye, Zhao Liu, Mingfei Sun, Bei Shi, Peilin Zhao, Hao Wu, Hongsheng Yu, Shaojie Yang, Xipeng Wu, Qingwei Guo, et al. Mastering complex control in moba games with deep reinforcement learning. In *Proceedings of the AAAI conference on artificial intelligence*, volume 34, pages 6672–6679, 2020. 6

[61] Yiming Gao, Bei Shi, Xueying Du, Liang Wang, Guangwei Chen, Zhenjie Lian, Fuhao Qiu, Guoan Han, Weixuan Wang, Deheng Ye, et al. Learning diverse policies in moba games via macro-goals. *Advances in Neural Information Processing Systems*, 34:16171–16182, 2021. 6

[62] Alexey Dosovitskiy, German Ros, Felipe Codevilla, Antonio Lopez, and Vladlen Koltun. Carla: An open urban driving simulator. In *Conference on robot learning*, pages 1–16. PMLR, 2017. 6, 7, 19

[63] Di Chen, Meixin Zhu, Hao Yang, Xuesong Wang, and Yinhai Wang. Data-driven traffic simulation: A comprehensive review. *IEEE Transactions on Intelligent Vehicles*, 2024. 6, 7, 21

[64] Hongyu Guo, Kun Xie, and Mehdi Keyvan-Ekbatani. Modeling driver’s evasive behavior during safety-critical lane changes: Two-dimensional time-to-collision and deep reinforcement learning. *Accident Analysis & Prevention*, 186:107063, 2023. 7, 21

[65] Suvin P Venthuruthiyil and Mallikarjuna Chunchu. Anticipated collision time (act): A two-dimensional surrogate safety indicator for trajectory-based proactive safety assessment. *Transportation research part C: emerging technologies*, 139:103655, 2022. 7, 21

[66] Samuel Sanford Shapiro and Martin B Wilk. An analysis of variance test for normality (complete samples). *Biometrika*, 52(3-4):591–611, 1965. 7, 21

[67] Nornadiah Mohd Razali, Yap Bee Wah, et al. Power comparisons of shapiro-wilk, kolmogorov-smirnov, lilliefors and anderson-darling tests. *Journal of statistical modeling and analytics*, 2(1):21–33, 2011. 7

[68] Leonid Nisonovich Vaserstein. Markov processes over denumerable products of spaces, describing large systems of automata. *Problemy Peredachi Informatsii*, 5(3):64–72, 1969. 7, 21

[69] Jens Beißenwenger. PDM-Lite: A rule-based planner for carla leaderboard 2.0. <https://github.com/0penDriveLab/DriveLM/blob/DriveLM-CARLA/docs/report.pdf>, 2024. Accessed: 2025-04-09. 7, 8, 9, 20, 21, 22, 24

[70] CARLA Team. CARLA Autonomous Driving Leaderboard. <https://leaderboard.carla.org/>, 2025. Accessed: 2025-04-09. 8, 18

[71] Katrin Renz, Kashyap Chitta, Otniel-Bogdan Mercea, A. Sophia Koepke, Zeynep Akata, and Andreas Geiger. Plant: Explainable planning transformers via object-level representations. In *Conference on Robotic Learning (CoRL)*, 2022. 8, 9, 22, 24

- [72] Peter E Hart, Nils J Nilsson, and Bertram Raphael. A formal basis for the heuristic determination of minimum cost paths. *IEEE Transactions on Systems Science and Cybernetics*, 4(2):100–107, 1968. [18](#)
- [73] Marco Cusumano-Towner, David Hafner, Alex Hertzberg, Brody Huval, Aleksei Petrenko, Eugene Vinitsky, Erik Wijmans, Taylor Killian, Stuart Bowers, Ozan Sener, et al. Robust autonomy emerges from self-play. [arXiv preprint arXiv:2502.03349](#), 2025. [20](#)
- [74] John Schulman, Philipp Moritz, Sergey Levine, Michael Jordan, and Pieter Abbeel. High-dimensional continuous control using generalized advantage estimation. [arXiv preprint arXiv:1506.02438](#), 2015. [21](#)

Appendix

A Theoretical Analysis	16
A.1 Problem Setup	16
A.2 Iterative Update in the Success-Probability Space	16
A.3 Existence of a Fixed Point	16
A.4 Uniqueness and Global Convergence	17
A.5 Detailed Proofs	17
B Experimental Details	18
B.1 Experiment Framework	18
B.2 CBV Identification Details	18
B.3 Algorithm Framework	19
B.4 Training Details	19
B.5 Baselines Detailed Description	19
B.6 State-Wise Reward Model Setup	20
B.7 Controllability and Realism Metrics	21
C AV Evaluation Details	22
C.1 AV Methods Implementation	22
C.2 AV Evaluation Metrics	22
D Additional Results	22
D.1 Detailed Qualitative Results of Controllability	22
D.2 Detailed Analysis in Driving Comfort	23
D.3 Visualization of the AV-Centered Closed-Loop Simulation	24
E Social Impact	25

A Theoretical Analysis

This section thoroughly analyzes *RIFT* under a binary reward setting ($r \in \{0, 1\}$) without any KL regularization. The dual-clip surrogate guarantees stable gradients and a globally convergent update in success-probability space.

A.1 Problem Setup

For a given state s , let $\pi_\theta(\tau \mid s)$ denote the probability of trajectory τ under policy parameters θ . Define the success probability

$$p_\theta(s) := \Pr_{\tau \sim \pi_\theta(\cdot \mid s)}(r(\tau, s) = 1),$$

and write $p := p_{\theta_{\text{old}}}(s) \in (0, 1)$ for the current policy. Since $r \in \{0, 1\}$, the mean and variance of the Bernoulli random variable are given by:

$$\mathbb{E}_{\tau \sim \pi_{\theta_{\text{old}}}}[r(\tau, s)] = p, \quad \text{Var}_{\tau \sim \pi_{\theta_{\text{old}}}}[r(\tau, s)] = p(1 - p).$$

The (group-)relative advantage [20] in Equation (6) therefore reduces to

$$\hat{A}(\tau, s) = \begin{cases} \sqrt{\frac{1-p}{p}}, & r(\tau, s) = 1, \\ -\sqrt{\frac{p}{1-p}}, & r(\tau, s) = 0. \end{cases} \quad (9)$$

Dual-Clip Surrogate. *RIFT* discards the KL term entirely and maximizes

$$f_\epsilon^{\text{RIFT}}(\rho_i, \hat{A}_i) = \max\left(\min(\rho_i \hat{A}_i, \text{clip}(\rho_i, 1 - \epsilon, 1 + \epsilon) \hat{A}_i), c \hat{A}_i\right), \quad (10)$$

where $\rho_i = \pi_\theta(\tau_i \mid s) / \pi_{\theta_{\text{old}}}(\tau_i \mid s)$ is the trajectory-level importance sampling ratio, $\epsilon > 0$ is the clipping range, and $c > 1$ caps the most negative value.

Remark A.1. If $\hat{A}_i < 0$ and $\rho_i \gg 1$, the naïve PPO/GRPO objective becomes a large negative value, producing unstable gradients. Because

$$f_\epsilon^{\text{RIFT}}(\rho_i, \hat{A}_i) \geq c \hat{A}_i, \quad (11)$$

the surrogate is never more negative than $c \hat{A}_i$, so

$$|\nabla_\theta \mathbb{E}[f_\epsilon^{\text{RIFT}}]| \leq |\nabla_\theta \mathbb{E}[\rho_i \hat{A}_i]|. \quad (12)$$

Hence, dual-clip reduces the worst-case gradient magnitude, ensuring stability.

A.2 Iterative Update in the Success-Probability Space

Let $\theta_{\text{new}} \in \arg \max_\theta \mathbb{E}_{\tau \sim \pi_{\theta_{\text{old}}}}[f_\epsilon^{\text{RIFT}}(\rho_i, \hat{A}_i)]$ and denote the corresponding success probability by $p_{\text{new}} := p_{\theta_{\text{new}}}(s)$. The update may therefore be viewed as a mapping

$$p_n = h_\epsilon(p_{n-1}), \quad (13)$$

with $p_{n-1} = p_{\theta_{\text{old}}}(s)$ and $p_n = p_{\text{new}}$. We prove:

- (i) $h_\epsilon : [0, 1] \rightarrow (0, 1)$ is well-defined and continuous;
- (ii) with suitable (c, ϵ) or a sufficiently small step size, h_ϵ is a contraction, yielding a unique fixed point $p^* \in (0, 1)$ and global convergence $p_n \rightarrow p^*$.

A.3 Existence of a Fixed Point

Lemma A.2 (Continuity and Interval Mapping). *For every $p \in [0, 1]$ the updated probability $h_\epsilon(p)$ lies in $(0, 1)$, and h_ϵ is continuous on $[0, 1]$.*

Proposition A.3 (Existence). *At least one fixed point $p^* \in (0, 1)$ satisfies $p^* = h_\epsilon(p^*)$.*

A.4 Uniqueness and Global Convergence

Bounded derivatives. For $\hat{A}_i \geq 0$, $|\partial f_\epsilon^{\text{RIFT}} / \partial \rho_i| \leq (1 + \epsilon) |\hat{A}_i|$; for $\hat{A}_i < 0$ it is bounded by $|\hat{A}_i|$. Consequently, the dependence of p_{new} on p admits a global Lipschitz constant $L(c, \epsilon)$.

Contraction. If $L(c, \epsilon) < 1$ or a step size $\eta < 1/L(c, \epsilon)$ is used, h_ϵ is a strict contraction on $(0, 1)$.

Theorem A.4 (Convergence of RIFT). *Assume $c > 1$ and $\epsilon > 0$. If $|h_\epsilon(p) - h_\epsilon(p')| \leq \lambda |p - p'|$ for some $\lambda < 1$ and all $p, p' \in (0, 1)$ —for example, by choosing a step size $\eta < 1/L(c, \epsilon)$ —then*

- (a) h_ϵ possesses a unique fixed point $p^* \in (0, 1)$;
- (b) any sequence $p_n = h_\epsilon(p_{n-1})$ converges geometrically: $|p_n - p^*| \leq \lambda^n |p_0 - p^*|$;
- (c) The dual-clip term eliminates gradient explosions caused by negative advantages, guaranteeing stable learning.

A.5 Detailed Proofs

Throughout this subsection, we reuse the notation introduced in Appendix A.4:

$$A^+(p) = \sqrt{\frac{1-p}{p}}, \quad A^-(p) = -\sqrt{\frac{p}{1-p}}, \quad \rho^+ = 1 + \epsilon, \quad \rho^- = 1 - \epsilon, \quad p \in (0, 1), \quad \epsilon > 0, \quad c > 1.$$

Proof of Lemma A.2. The proof consists of three parts.

Boundary points. If $p = 0$, every trajectory under the old policy fails and $A^+(0^+) = \infty$. For any candidate new policy with success probability $q \in (0, 1]$,

$$\mathcal{J}(q) = q \rho^+ A^+(0^+) + (1 - q) c A^-(0^+) = (1 + \epsilon) q \cdot \infty > 0, \quad \mathcal{J}(0) = 0.$$

Hence $h_\epsilon(0) = \arg \max_q \mathcal{J}(q) > 0$. The case $p = 1$ is symmetric, yielding $h_\epsilon(1) < 1$.

Interior points. Let $p \in (0, 1)$ and denote the step in parameter space by $\Delta\theta$. Smoothness of $\theta \mapsto \pi_\theta$ implies $|\log \rho_i| \leq K \|\Delta\theta\|$ for some $K < \infty$. Because f_ϵ^{RIFT} is $(1 + \epsilon)$ -Lipschitz in ρ_i , the expected surrogate, cannot change by more than $K(1 + \epsilon) \|\Delta\theta\|$ in one update; choosing $\|\Delta\theta\| < (K(1 + \epsilon))^{-1}$ keeps $h_\epsilon(p)$ strictly inside $(0, 1)$.

Continuity. Set $\Psi(\theta, p) = \mathbb{E}_{\tau \sim \pi_\theta}[f_\epsilon^{\text{RIFT}}]$. Joint continuity of Ψ and compactness of the trajectory space (after clipping) satisfies the hypotheses of Berge's maximum theorem, so the maximizer correspondence $\arg \max_\theta \Psi(\theta, p)$ is upper-hemicontinuous; the composition yields continuity of h_ϵ on $[0, 1]$. \square

Proof of Proposition A.3. Define $g(p) = h_\epsilon(p) - p$. Lemma A.2 gives $g(0) > 0$ and $g(1) < 0$, while Lemma A.2 also guarantees the continuity of g . The Intermediate Value Theorem therefore yields a root $p^* \in (0, 1)$ with $p^* = h_\epsilon(p^*)$. \square

Proof of Theorem A.4. The proof proceeds in four steps.

Step 1 – maximized surrogate. Substituting ρ^+, ρ^- into the surrogate gives

$$\Phi(p) = p \rho^+ A^+(p) + (1 - p) \rho^- A^-(p) = 2\epsilon \sqrt{p(1-p)}. \quad (14)$$

Step 2 – Lipschitz bound.

$$\Phi'(p) = \epsilon \frac{1 - 2p}{\sqrt{p(1-p)}}, \quad |\Phi'(p)| \leq \frac{\epsilon}{\sqrt{p(1-p)}}. \quad (15)$$

Fix $\delta \in (0, \frac{1}{2})$ such that the first iterate satisfies $h_\epsilon(p_0) \in [\delta, 1 - \delta]$ (Lemma A.2 ensures such a δ exists). Then $|\Phi'(p)| \leq L_\delta(\epsilon) := \epsilon / \sqrt{\delta(1-\delta)}$ for every subsequent p .

Step 3 – contraction. Using a gradient step $p_n = p_{n-1} + \eta \Phi'(p_{n-1})$ with $\eta \in (0, 1/L_\delta(\epsilon))$ gives

$$|p_n - p_{n-1}| \leq \eta L_\delta(\epsilon) |p_{n-1} - p_{n-2}| =: \lambda |p_{n-1} - p_{n-2}|, \quad \lambda < 1. \quad (16)$$

Thus h_ϵ is a strict contraction on $([\delta, 1 - \delta], |\cdot|)$.

Step 4 – Banach fixed-point theorem. Because the metric space $([\delta, 1 - \delta], |\cdot|)$ is complete and h_ϵ is a strict contraction on it, Banach's fixed-point theorem guarantees

(a) the existence and uniqueness of a fixed point $p^* \in (\delta, 1 - \delta) \subset (0, 1)$ such that $p^* = h_\epsilon(p^*)$;

(b) geometric convergence of the iterates generated by $p_n = h_\epsilon(p_{n-1})$:

$$|p_n - p^*| \leq \lambda^n |p_0 - p^*|, \quad 0 < \lambda < 1. \quad (17)$$

Step 5 – bounded negative-advantage gradients. For every $\hat{A}_i < 0$

$$f_\epsilon^{\text{RIFT}}(\rho_i, \hat{A}_i) = \max(\min(\rho_i \hat{A}_i, \rho^- \hat{A}_i), c \hat{A}_i) \geq c \hat{A}_i, \quad (18)$$

so $|\partial f_\epsilon^{\text{RIFT}} / \partial \rho_i| \leq |\hat{A}_i|$, preventing gradient explosions and guaranteeing stability. \square

B Experimental Details

B.1 Experiment Framework

To enable reliable AV-centered closed-loop simulation, we develop our framework based on widely adopted closed-loop traffic simulation platforms, such as the CARLA Leaderboard [70] and Bench2Drive [46]. Traditionally, these platforms use predefined scenarios along the AV's global route to evaluate the multi-dimensional performance of AV methods. In contrast, we replace these static scenarios with dynamically generated traffic flows by randomly spawning background vehicles around the AV's global path and simulating their behavior using rule-based driving policies, as described in Section 3.1. Through the CBV identification mechanism outlined in Appendix B.2, we naturally introduce interactions between the AV and CBVs, thereby generating continuous, interactive scenarios over time. This framework serves as the foundation for both the training and evaluation processes in this paper.

B.2 CBV Identification Details

Identifying Critical Background Vehicles (CBVs) is essential to our AV-centered closed-loop simulation. Let \mathcal{V}_{AV} denote the autonomous vehicle (AV), and $\mathcal{V}_{\text{BV}} = \{\mathcal{V}_i\}_{i=1}^N$ represent the set of background vehicles in the environment. The AV navigates along a predefined global route $\mathcal{P} = \{p_k\}_{k=1}^M$, where each p_k corresponds to a waypoint along the route. The goal of CBV identification is to select background vehicles that are likely to share the AV's destination and have similar estimated travel distance, thereby facilitating route-level interactions between the AV and CBVs. The primary criterion for identifying CBVs is the relative *distance-to-goal* difference between the AV and each background vehicle. This is mathematically expressed as:

$$\left| \hat{D}_{\text{global}}(p_k, \mathcal{V}_i) - \hat{D}_{\text{global}}(p_k, \mathcal{V}_{\text{AV}}) \right| < \delta, \quad (19)$$

where, $\hat{D}_{\text{global}}(p_k, \mathcal{V}_i)$ and $\hat{D}_{\text{global}}(p_k, \mathcal{V}_{\text{AV}})$ denote the estimated travel distance required for the background vehicle \mathcal{V}_i and the AV to reach waypoint p_k , respectively. The distance-to-goal for each vehicle is computed by determining the distance from its current position to the target waypoint p_k using the A* global path planning algorithm [72]. A threshold δ is introduced to define the maximum allowable difference in distance-to-goal. A background vehicle is considered critical and included in the CBV set \mathcal{C} if the absolute distance-to-goal difference between it and the AV is smaller than δ .

This approach selects background vehicles whose destinations and estimated travel distances are sufficiently aligned with those of the AV, thereby ensuring meaningful and realistic route-level interactions. Once a CBV is identified, the planning path previously generated via A* during distance-to-goal estimation is directly adopted as its global navigation path, naturally introducing route-level interactions between the AV and CBVs. The threshold δ serves as a tunable parameter to adjust the sensitivity of the CBV selection process. In this study, we set δ to 15m to achieve a balanced trade-off between sensitivity and selection accuracy.

B.3 Algorithm Framework

For clarity, we summarize the procedure of *RIFT* within our AV-centered closed-loop simulation framework in Algorithm 1. The trajectory generation model initializes from the IL pre-trained checkpoint provided by Pluto official codebase¹, followed by closed-loop RL fine-tuning within the CARLA simulator [62] to generate realistic and controllable traffic scenarios.

Algorithm 1 Procedure for *RIFT* in the AV-Centered Closed-Loop Simulation Framework.

```

1: Input: IL pre-trained trajectory generation model  $\pi_{\theta_{\text{init}}}$ , buffer  $\mathcal{D}$   $\triangleright$  IL pre-training (nuPlan [11])
2: trajectory generation model  $\pi_{\theta} \leftarrow \pi_{\theta_{\text{init}}}$ 
3: for iteration = 1, ...,  $I$  do  $\triangleright$  Closed-loop RL fine-tuning (CARLA [62])
4:   Update the old trajectory generation model  $\pi_{\theta_{\text{old}}} \leftarrow \pi_{\theta}$ 
5:   while  $\mathcal{D}$  not full do  $\triangleright$  Collect rollout data
6:     for step = 1, ...,  $T$  do
7:       Generate  $G$  trajectories  $\{\tau_i\}_{i=1}^G \sim \pi_{\theta_{\text{old}}}$  for each CBV  $\triangleright$  Policy inference
8:       Compute reward  $\{r_i\}_{i=1}^G$ , advantage  $\{\hat{A}_i\}_{i=1}^G$  for each trajectory  $\tau_i$  with Equation (6)
9:       Store transition into buffer  $\mathcal{D}$ 
10:    end for
11:   end while
12:   for RIFT iteration = 1, ...,  $\mu$  do  $\triangleright$  Policy fine-tuning
13:     Sample mini-batches transition from the buffer  $\mathcal{D}$ 
14:     Update model  $\pi_{\theta}$  by maximizing the RIFT objective (Equation (8))
15:   end for
16: end for
17: Output: RL fine-tuned trajectory generation model

```

B.4 Training Details

We perform closed-loop fine-tuning on selected modules of the IL pre-trained trajectory generation model (Pluto). As shown in the ablation results (Section 5.4), fine-tuning only the trajectory scoring head achieves the best trade-off between realism and controllability. Accordingly, all fine-tuning baselines adopt this setting to ensure consistency and fair comparison. Our training framework is built on the open-source Lightning platform². Fine-tuning is conducted on $2 \times$ Bench2Drive220, while evaluation is performed on dev10, both from the Bench2Drive project. All experiments are conducted on NVIDIA GeForce RTX 4090D GPUs, with each fine-tuning run taking approximately 8 hours on a single GPU. Detailed training setups and hyperparameter configurations are provided in Table 4 and Table 5.

B.5 Baselines Detailed Description

To comprehensively evaluate *RIFT* in an AV-centered closed-loop simulation environment, we compare it against a range of baselines, including pure imitation learning (IL), pure reinforcement learning (RL), and various fine-tuning approaches based on IL, RL, or their combination. We initialize all fine-tuning methods from the pre-trained Pluto checkpoint and fine-tune only the trajectory scoring head to preserve trajectory-level realism. The details of each baseline are summarized below.

- *Pluto* [53] is an open-source IL-based planning framework for autonomous driving. It processes vectorized scene representations as input and outputs multimodal trajectories for downstream planning. In AV-centered closed-loop simulation, the method directly uses a pre-trained checkpoint without additional fine-tuning.
- *FREA* [14] is an RL-based approach designed to generate safety-critical yet AV-feasible scenarios. It incorporates a feasibility-aware training objective. In the AV-centered closed-loop simulation, FREA selects potential collision points along the AV’s global route as adversarial goals.

¹<https://github.com/jchengai/pluto>

²<https://github.com/Lightning-AI/pytorch-lightning>

- *PPO* [14] is a variant of FREA that focuses solely on generating safety-critical scenarios. Unlike FREA, it disregards the feasibility constraints of AV and treats adversariality as the only optimization objective.
- *FPPO-RS* [14] is another FREA variant that integrates AV’s feasibility constraints into the reward shaping process, thereby balancing adversariality with scenario reasonability.
- *PPO-Pluto* fine-tunes the pre-trained trajectory generation model using the PPO algorithm [58]. The fine-tuning follows the same reward structure as detailed in Appendix B.6, aligning with *RIFT*.
- *REINFORCE-Pluto* employs the REINFORCE algorithm [59] to fine-tune the pre-trained Pluto model under the same reward design as detailed in Appendix B.6.
- *GRPO-Pluto* utilizes the basic GRPO algorithm [20] for fine-tuning, employing the pre-trained Pluto model as the reference for KL regularization, while incorporating the standard PPO-Clip.
- *SFT-Pluto* is a purely supervised fine-tuning approach, where PDM-Lite [69] serves as the expert model, providing supervision at the target speed level.
- *RTR-Pluto* [21] is a hybrid framework combining imitation and reinforcement learning. While the original RTR utilizes human driving trajectories as supervision, our setting replaces this with PDM-Lite due to the lack of human-level demonstrations. The RL component uses sparse infraction-based rewards, consistent with the original RTR, and applies PPO for optimization.
- *RS-Pluto* [22] also adopts a hybrid IL+RL paradigm, originally trained via REINFORCE using ground-truth supervision and sparse rewards to ensure safety and realism. In our adaptation, PDM-Lite substitutes the ground-truth expert, while the rest of the methodology remains unchanged.

B.6 State-Wise Reward Model Setup

To capture diverse human driving styles, we decompose driving behaviors into distinct reward components, following [73]. Different styles are constructed by combining weights assigned to each reward component (detailed in Table 6), enabling a range of behaviors from aggressive to conservative. The total driving reward is defined as:

$$R = R_{\text{collision}} + R_{\text{off-road}} + R_{\text{comfort}} + R_{\text{lane}} + R_{\text{velocity}} + R_{\text{timestep}}. \quad (20)$$

The individual terms are described as follows:

- $R_{\text{collision}} = -(\alpha_{\text{collision}} + |v|) \mathbb{1}_{\text{collision}}$: penalizes collisions, with higher penalties at higher speeds.
- $R_{\text{off-road}} = -\alpha_{\text{boundary}} \mathbb{1}_{\text{boundary}}$: penalizes deviations from the drivable area.
- $R_{\text{comfort}} = -\alpha_{\text{comfort}} (\mathbb{1}_{|a|>4} + \mathbb{1}_{|\omega|>4})$ penalizes excessive acceleration and angular acceleration.
- $R_{\text{l-align}} = \alpha_{\text{l-align}} (\min(\cos(\theta_f), 0) + \alpha_{\text{vel-align}} \min(\cos(\theta_f) * v, 0) + 0.25 (1 - \frac{|\theta_f|}{\pi/2}))$: guides the agent to follow the correct driving direction and remain parallel to the lane markings.
- $R_{\text{l-center}} = -\alpha_{\text{l-center}} (\mathbb{1}_{\cos(\theta_f)>0.5} * \left(|x_f - \alpha_{\text{center-bias}}| - \frac{0.05}{\exp(|x_f - \alpha_{\text{center-bias}}| - 0.5)} \right))$: guides the agent to prefer trajectories that remain centered within the lane.
- $R_{\text{velocity}} = \alpha_{\text{velocity}} \max(\cos(\theta_f), 0.0) \mathbb{1}_{3<|v|<20} * |v|$: promotes forward movement and biases the agent toward choosing routes with consistent traffic flow rather than traffic jams.
- $R_{\text{timestep}} = -\alpha_{\text{timestep}} \mathbb{1}_{|v|>0 \vee |a|>0}$ applies a small per-step penalty, encouraging efficiency. It is disabled when the agent is stationary to allow appropriate waiting behavior at intersections.

Building on the reward definitions above, we construct a state-wise reward model *StateWiseRM*(\cdot), which computes a scalar reward based on a set of interpretable features extracted from each trajectory point τ_i^t . Specifically, we define a feature extraction function $\phi(\tau_i^t)$ as:

$$\phi(\tau_i^t) = (\mathbb{1}_{\text{collision}}, \mathbb{1}_{\text{boundary}}, a_{\text{long}}, a_{\text{lat}}, \theta_f, x_f, v, a), \quad (21)$$

where:

- $\mathbb{1}_{\text{collision}}$ and $\mathbb{1}_{\text{boundary}}$ are binary indicators of potential collisions and off-road violations;
- a_{long} and a_{lat} denote the longitudinal and lateral acceleration;

Table 4: Hyperparameters used in *RIFT* Training.

Parameter	Value
Batch size	256
Rollout buffer capacity	4096
Fine-tune initial LR	$1 \times e^{-4}$
Minimum LR	$1 \times e^{-6}$
LR decay across iteration	0.9
LR schedule	Cosine
Num. RIFT epoch	16
Warmup Epoch of RIFT	3
AdamW weight-decay	$1 \times e^{-5}$

Table 5: Hyperparameters of *RIFT* or RL baselines.

Parameter	Value
PPO clipping ratio ϵ	0.2
Dual-clip ratio c	3
Discount factor γ	0.98
λ_{GAE} [74]	0.98
Hidden dimension D	128
Num. lon. queries N_{lon}	12
Traj. time horizon T	80
Map radius	120m
Frame rate	10Hz

Table 6: Reward Parameters for Different Driving Styles.

Parameter	Normal	Aggressive
$\alpha_{\text{collision}}$	20.0	5.0
α_{boundary}	5.0	5.0
α_{comfort}	0.8	0.8
$\alpha_{\text{l-align}}$	0.5	0.5
$\alpha_{\text{vel-align}}$	0.05	0.05
$\alpha_{\text{l-center}}$	0.6	0.6
$\alpha_{\text{center-bias}}$	0.0	0.0
α_{velocity}	0.1	0.2
α_{timestep}	0.1	0.1

- v and a are the magnitudes of velocity and acceleration;
- x_f is the lateral distance to the nearest lane centerline;
- θ_f is the heading deviation with respect to the lane direction.

The state-wise reward is then computed as:

$$r_i^t = \text{StateWiseRM}(\phi(\tau_i^t)). \quad (22)$$

All features, except the infraction indicators, are directly derived from the trajectory. To estimate future infractions, we follow the forecasting model in [69] to simulate other agents' future positions based on current states and actions and identify collisions via bounding box overlap. Off-road violations are detected using the Euclidean Signed Distance Field (ESDF) [53].

B.7 Controllability and Realism Metrics

Controllability. Following the metric design principles proposed in the WOSAC challenge [34] and other widely adopted evaluation frameworks [42, 63], we adopt a set of well-established metrics to comprehensively assess different aspects of controllability:

- *Scenario Collision Per Kilometer (CPK)* [63]: the average number of scenario collisions per kilometer of driving distance.
- *Off-Road Rate (ORR)* [63]: the percentage of time that CBVs spend off-road on average.
- *Route Progress (RP)* [63]: the total distance traveled by all CBVs, reflecting route completion.
- *2D Time-to-Collision (2D-TTC)* [64]: the minimum of longitudinal and lateral time-to-collision from the AV's perspective, capturing the immediate interaction risk posed by CBVs.
- *Anticipated Collision Time (ACT)* [65]: a safety-critical metric measuring the AV's proximity to potential collisions, reflecting the interaction intensity introduced by CBVs.

Realism. Following [63], most realism metrics rely on ground-truth trajectories of human drivers to evaluate how closely simulation agents mimic real-world behavior. However, since all our experiments are conducted in the CARLA simulator without expert demonstrations, we adopt distribution-level metrics to assess the realism of CBV behavior in terms of speed and acceleration. Specifically, we employ the following two metrics:

- *Wasserstein Distance (WD)* [68]: measures the distance between two distributions μ and ν . Since CARLA provides a predefined target speed for agents, we use WD to compare the simulated CBV speed distribution with the target speed distribution as the reference.

$$\text{WD}(\mu, \nu) = \inf_{\gamma \in \Pi(\mu, \nu)} \mathbb{E}_{(x, y) \sim \gamma} [d(x, y)]. \quad (23)$$

- *Shapiro–Wilk test (SW)* [66]: assesses whether the distribution of speed and acceleration follows a normal distribution, capturing the statistical naturalness of CBV motion.

$$\text{SW} = \frac{\left(\sum_{i=1}^n a_i x_{(i)} \right)^2}{\sum_{i=1}^n (x_i - \bar{x})^2}, \quad (24)$$

where a_i are coefficients, $x_{(i)}$ are the ordered data points, x_i are the sample values, \bar{x} is the sample mean, and n is the number of data points.

C AV Evaluation Details

C.1 AV Methods Implementation

To assess the effectiveness of *RIFT* in generating reliable and interactive scenarios for AV evaluation in the AV-centered closed-loop simulation environment, we evaluate the following representative and stable AV methods:

- *PDM-Lite* [69]: A rule-based privileged expert method that achieves state-of-the-art performance on the CARLA Leaderboard 2.0 by leveraging components such as the Intelligent Driver Model and the kinematic bicycle model. This open-source method serves as a strong baseline for comparison.
- *PlanT* [71]: An explainable, learning-based planning method that operates on an object-level input representation and is trained through imitation learning.

C.2 AV Evaluation Metrics

As detailed in Appendices B.1 and B.4, we develop an AV-centered closed-loop simulation environment, including a training and evaluation pipeline based on Bench2Drive. The AV closed-loop evaluation metrics proposed in Bench2Drive extend the original metrics of the CARLA Leaderboard by emphasizing the specific strengths and weaknesses of different methods across various aspects, such as merging and overtaking, thereby making them suitable for evaluating performance under predefined scenarios. However, as noted in Appendix B.1, replacing predefined scenarios with CBV-generated traffic flows precludes the evaluation of specific AV capabilities. Since our primary objective is to validate the effectiveness of *RIFT* in providing reliable traffic scenarios for AV evaluation, we follow the default evaluation metrics from CARLA Leaderboard to assess the overall driving performance of the AV. Additionally, we introduce a new metric to quantify the AV blockage events, which may arise when traffic flows are unreliable. The evaluation metrics are summarized as follows:

- *Driving Score (DS)*: $R_i P_i$ — The main metric of the leaderboard, calculated as the product of route completion and the infraction penalty. Here, R_i represents the percentage of completion of the i -th route, and P_i denotes the infraction penalty. The maximum value is 100.
- *Route Completion (RC)*: R_i — The percentage of the route distance completed by the agent. The maximum value is 100.
- *Infraction penalty (IP)*: $P_i = \prod_j p_j^{\text{infractions}_j}$ — This metric tracks various types of infractions and aggregates all instances triggered by the agent as a geometric series. The agent starts with an ideal base score of 1.0, which decreases with each infraction to a minimum of 0.
- *Block Rate (BR)*: The average number of occurrences where a CBV fails to navigate its route normally and obstructs the AV’s progress.

D Additional Results

D.1 Detailed Qualitative Results of Controllability

As discussed in Section 5.4, we investigate the controllability of *RIFT* under different reward configurations. The aggressive variant applies a reduced collision penalty and places greater emphasis on driving efficiency (Table 6), encouraging assertive behaviors such as overtaking. In contrast, the normal configuration imposes a higher collision penalty to promote safer and more conservative driving behaviors.

Quantitative results in Table 3 show that the aggressive variant achieves higher Progress and Speed Realism scores, albeit at the cost of increased infractions. To complement these findings, Figure 6 presents a qualitative comparison in a single-lane intersection scenario where a leading BV halts at a stop sign. The aggressive CBV variant attempts an overtaking maneuver, resulting in a collision,

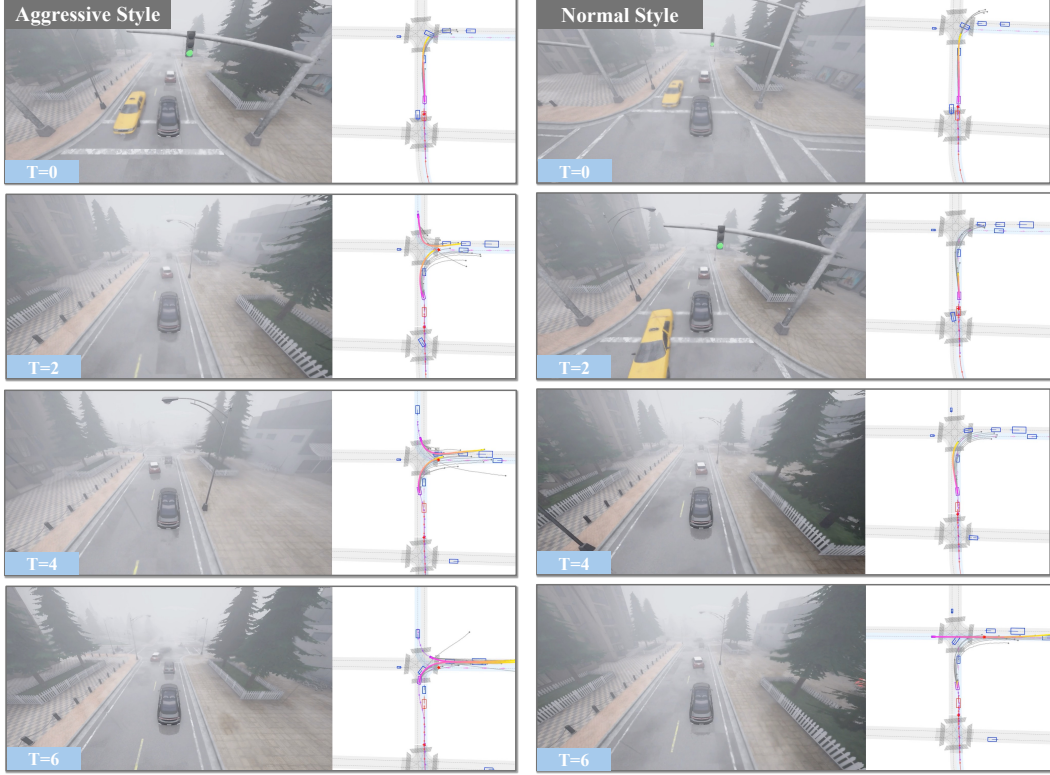


Figure 6: Qualitative illustration of *RIFT*'s controllability under different reward configurations. CBV is marked in purple, AV (PDM-Lite) is in red, and BVs are in blue.

whereas the normal CBV variant yields and waits, demonstrating distinct behavioral patterns induced by different reward preferences. These results highlight the controllability of *RIFT* in modulating driving behaviors according to user-specified reward configurations.

D.2 Detailed Analysis in Driving Comfort

Metrics. To further evaluate the driving comfort of different CBV methods, we define several comfort metrics based on Bench2Drive, which assesses agent comfort through acceleration and jerk profiles. Specifically, we measure comfort using the following metrics:

- *Uncomfortable Rate (UCR)*: the percentage of simulation time during which CBVs experience discomfort.
- *Driving Jerk (Jerk)*: the time derivative of acceleration, quantifying the abruptness of acceleration changes and the smoothness of CBV trajectories.

To determine whether a CBV's current state is considered comfortable, we adopt the Frame Variable Smoothness (FVS) criterion from Bench2Drive:

$$\text{Frame Variable Smoothness (FVS)} = \begin{cases} \text{True} & \text{if lower bound} \leq p_i \leq \text{upper bound}. \\ \text{False} & \text{otherwise} \end{cases} \quad (25)$$

$p \in \text{smoothness vars}, 0 \leq i \leq \text{total frames}$

The smoothness variables include longitudinal acceleration (expert bounds: [-4.05, 2.40]), maximum absolute lateral acceleration (expert bounds: [-4.89, 4.89]), and maximum jerk magnitude (expert bounds: [-8.37, 8.37]).

Main Results. The quantitative results of the comfort metrics are presented in Table 7. All CBV methods exhibit notable levels of driving discomfort. Although the more conservative methods identified in Section 5.2 achieve relatively lower discomfort levels, a high baseline of discomfort persists across methods.

Table 7: **Comparison of CBV Comfort Metrics across various AV Methods.** Each metric is evaluated across three random seeds.

Method	PDM-Lite [69]		PlanT [71]	
	UCR ↓	Jerk ↓	UCR ↓	Jerk ↓
Pluto [53]	56.45 ± 4.14	-0.16 ± 3.72	50.26 ± 2.17	-0.42 ± 3.38
PPO [14]	74.76 ± 2.71	-0.51 ± 4.61	74.90 ± 1.21	0.40 ± 4.83
FREA [14]	72.40 ± 1.72	0.29 ± 4.61	73.48 ± 3.83	-0.15 ± 4.91
FFPO-RS [14]	68.33 ± 1.90	-0.07 ± 3.96	66.67 ± 0.82	-0.15 ± 3.95
SFT-Pluto	68.14 ± 4.91	-0.06 ± 4.06	59.78 ± 4.72	-0.11 ± 4.00
RS-Pluto [22]	70.31 ± 4.07	0.32 ± 4.12	65.18 ± 2.11	-0.16 ± 4.07
RTR-Pluto [21]	55.58 ± 4.76	-0.19 ± 3.37	45.12 ± 2.66	-0.14 ± 3.34
PPO-Pluto	58.29 ± 2.70	-0.32 ± 3.70	54.85 ± 5.82	-0.07 ± 3.40
REINFORCE-Pluto	68.10 ± 1.22	0.23 ± 3.96	64.94 ± 5.36	-0.11 ± 3.96
GRPO-Pluto	78.58 ± 0.59	0.22 ± 4.62	77.13 ± 0.65	-0.23 ± 4.58
<i>RIFT</i> -Pluto (ours)	76.90 ± 2.82	0.59 ± 4.12	72.41 ± 4.02	0.21 ± 4.44

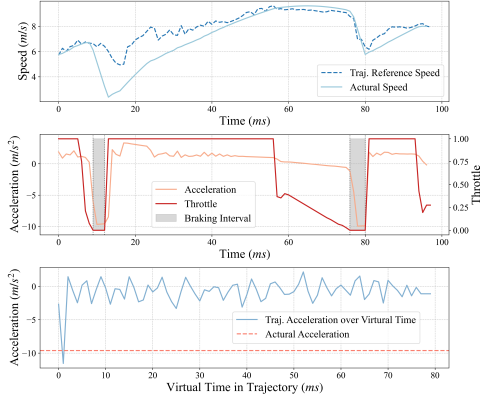


Figure 7: Controller Performance.

To investigate the underlying causes of discomfort, we further decouple the planned trajectories from the executed control actions. In CARLA, most CBV methods rely on PID controllers to transform high-level trajectory waypoints into executable driving commands, including throttle, steering, and brake. As shown in Figure 7, the upper panel illustrates the speed tracking curve, while the middle panel presents the raw throttle signal and corresponding acceleration profile.

Because trajectory generation is performed state-wise—predicting only the immediate next action—the reference speed may vary discontinuously over time. These discontinuities are amplified by the PID controller, whose binary throttle/brake responses induce abrupt changes in acceleration, ultimately leading to discomfort during vehicle operation. Such execution-level instabilities are a major contributor to the discomfort observed across CBV methods.

While many CBV methods attempt to mitigate discomfort through fine-tuning strategies that incorporate post-action feedback via reward shaping or expert action alignment—*RIFT* adopts a different approach. It employs a state-wise reward model (see Appendix B.6) that quantifies comfort within the trajectory’s virtual time domain.

To further analyze this, we visualize both the actual acceleration after executing a selected trajectory and the corresponding virtual-time acceleration (shown in Figure 7). The results reveal that while virtual-time acceleration aligns with actual motion at the beginning of the trajectory, it underestimates acceleration variations in later segments. This leads to an overly conservative estimation of trajectory-level discomfort, resulting in insufficient supervision during training and reflected in *RIFT*’s comfort performance in Table 7.

In summary, the discomfort exhibited by CBV methods can be attributed to two primary sources:

- **Tracking instability**, caused by discontinuities in planned trajectories and the limited control fidelity of PID controllers. Discrete, state-wise planning combined with low-resolution, often binary control outputs amplifies acceleration fluctuations and leads to uncomfortable motion.
- **Inadequate comfort modeling**, particularly in state-wise reward formulations such as that adopted by *RIFT* and GPRO. These formulations fail to capture long-term trajectory-level discomfort, leading to insufficient supervision during training and suboptimal comfort performance.

D.3 Visualization of the AV-Centered Closed-Loop Simulation

To qualitatively evaluate the robustness of *RIFT* across diverse AV-centered scenarios, we provide additional temporal visualizations of closed-loop simulations. As shown in Figure 8, the traffic scene consists of the autonomous vehicle (AV, controlled by PDM-Lite), background vehicles (BVs), and critical background vehicles (CBVs), which interact dynamically over time.

The visualizations demonstrate the ability of *RIFT* to generate temporally coherent, realistic, and controllable trajectories across a variety of traffic situations. Even under complex and evolving closed-loop conditions, *RIFT* maintains stable multimodal behavior, highlighting its effectiveness in simulating realistic and controllable traffic flows around the AV.

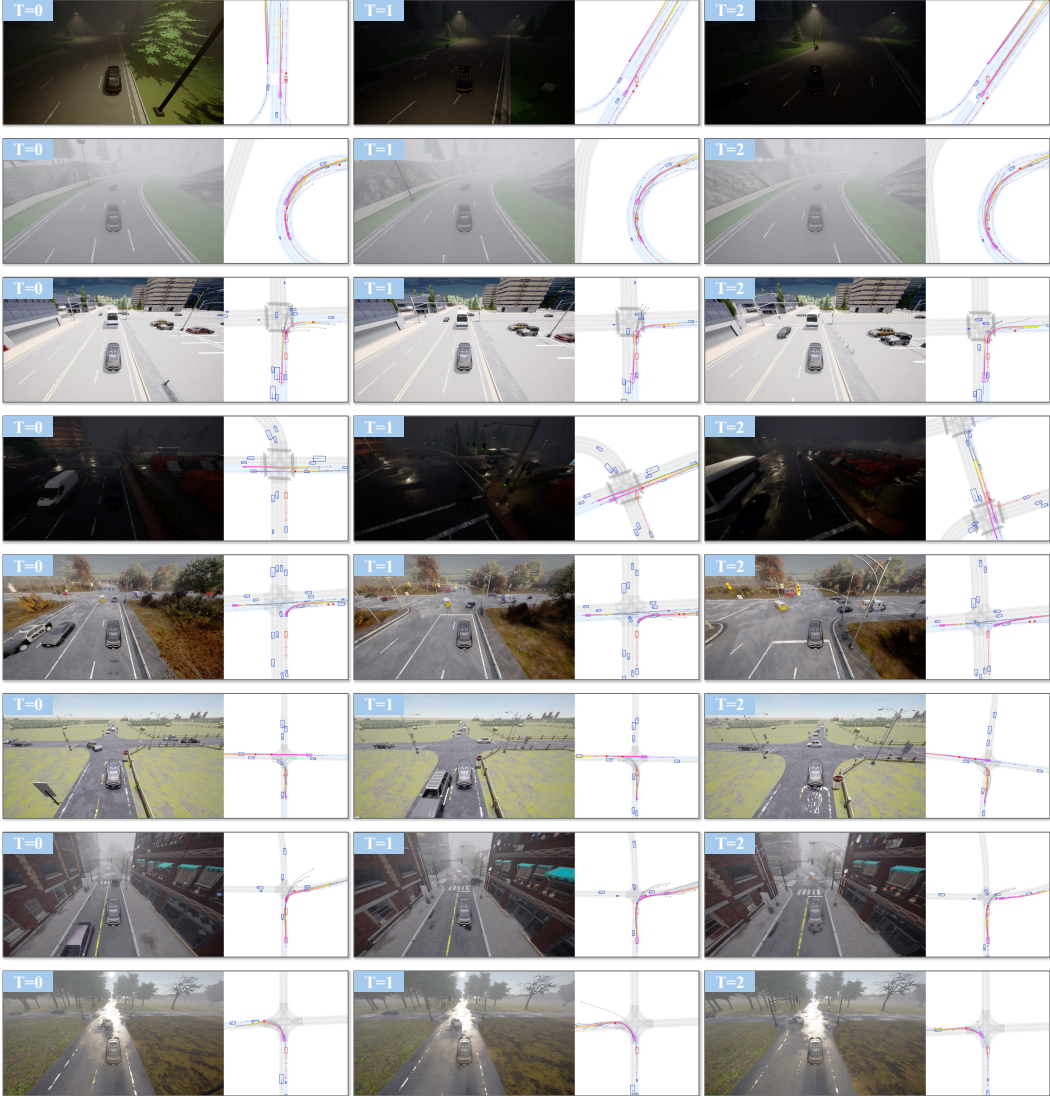


Figure 8: Extra temporal visualization of *RIFT* in the AV-centered closed-loop simulation environment. CBV is marked in purple, AV (PDM-Lite) is in red, and BVs are in blue.

E Social Impact

Positive Societal Impacts. This work introduces a practical framework that bridges realism and controllability in traffic simulation. By decoupling the pre-training and fine-tuning stages, our method enables models pre-trained on real-world datasets to be effectively adapted to physics-based simulators, preserving trajectory-level realism while improving long-horizon, closed-loop performance. This paradigm offers a viable path for data-driven approaches to transition toward physics-based simulators, facilitating more reliable closed-loop testing and training. Consequently, it contributes to the development of safer and more robust autonomous systems.

Negative Societal Impacts. While fine-tuning in physics-based simulators improves closed-loop performance, it may also lead to overfitting to the specific characteristics of the simulator. As a result, the learned policy could struggle to generalize beyond the simulated environment, giving rise to a sim-to-real gap. This gap poses challenges for real-world deployment, as models that perform well in simulation may not retain the same level of reliability when applied to actual autonomous driving systems. Such discrepancies can affect the testing and training stages, highlighting the need for further work to ensure real-world transferability.